

Continuation with Non-invasive Control Schemes: Revealing Unstable States in a Pedestrian Evacuation Scenario*

Ilias Panagiotopoulos[†], Jens Starke[‡], Jan Sieber[§], and Wolfram Just[¶]

Abstract.

This paper presents a framework to perform bifurcation analysis in laboratory experiments or simulations. We employ *control-based continuation* to study the dynamics of a macroscopic variable of a microscopically defined model, exploring the potential viability of the underlying feedback control techniques in an experiment. In contrast to previous experimental studies that used iterative root-finding methods on the feedback control targets, we propose a feedback control law that is inherently non-invasive. That is, the control discovers the location of equilibria and stabilizes them simultaneously. We call the proposed control *zero-in-equilibrium feedback control* and we prove that it is able to stabilize branches of equilibria, except at singularities of codimension $n + 1$, where n is the number of state space dimensions the feedback can depend on.

We apply the method to a simulated evacuation scenario where pedestrians have to reach an exit after maneuvering left or right around an obstacle. The scenario shows a hysteresis phenomenon with bistability and tipping between two possible steady pedestrian flows in microscopic simulations. We demonstrate for the evacuation scenario that the proposed control law is able to uniformly discover and stabilize steady flows along the entire branch, including points where other non-invasive approaches to feedback control become singular.

Key words. multistability, bifurcation analysis, pedestrian flow, control-based continuation, non-invasive control, feedback control, unstable states in experiments

AMS subject classifications. 68Q25, 68R10, 68U05

1. Introduction. The analysis of systems involving many interacting microscopic components is often desired in terms of a few, macroscopic quantities, such as averages over all components [14]. Qualitative behavior, such as the system being in equilibrium or whether it shows multistability or is near a tipping point, are expressed at this macroscopic level [33]. However, the derivation of a model for the evolution of the macroscopic quantities typically relies on assumptions that are not realistic or are known to introduce a bias. For example in networks, mean-field equations rely on closure approximations. These closures assume absence of correlations beyond a fixed diameter, for practical reasons this diameter equals 1 such that one ignores correlations beyond nearest neighbors [16, 17, 29, 23]. On the other hand, a microscopic model may well be amenable to direct simulations (from which one can extract macroscopic quantities) and may be easy to connect to observed data or first principles, as its parameters encode the individual behavior of the interacting agents of the underlying system. Applications of direct simulations for individual-based models in ecology are discussed in [32].

We focus on an approach inspired by its applicability to experiments, providing a non-technical overview of in Section 2. The engineering and physics communities have independently developed feedback control laws that enable one to perform bifurcation analysis directly

*Submitted to the editors DATE.

[†]Institute of Mathematics, University of Rostock, Germany.

[‡]Institute of Mathematics, University of Rostock, Germany.

[§]College of Engineering, Mathematics and Physical Sciences, University of Exeter, United Kingdom.

[¶]School of Mathematical Science, Queen Mary University of London, United Kingdom.

on physical experiments [30, 43, 4]. In particular, these control-based methods can track dynamical phenomena that are either dynamically unstable or too sensitive to disturbances to be visible in uncontrolled experiments [35]. Section 3 will start with a brief review of methods for performing bifurcation analysis without deriving explicit equations, including our approach of using *non-invasive feedback control*.

Subsection 3.3 will reformulate one of the classical inherently non-invasive feedback laws, which are based on washout filters, in a way that makes it treatable with standard controllability arguments, which can be decided by the regularity or singularity of a controllability matrix. We then construct a new control law that removes all singularities, except for some events of high codimension along branches of equilibria.

We demonstrate the proposed methodology on a microscopically defined model, a particle flow model for pedestrians moving along a corridor past an obstacle, introduced in Section 4. Our control-based continuation of this scenario, which exhibits bistability and two tipping points at a macroscopic level, reveals the unstable pedestrian flows and completes a bifurcation diagram in Section 5 without the use of any macroscopic model. During our analysis, we assume all the limitations of a physical experiment and, thus, our approach can be extended to real life scenarios.

2. Non-technical overview. Let us assume that an experiment (computational or physical) can be described by an ordinary differential equation (ODE) with some state $x(t)$ and parameters μ from which the output originates in the form $y(t) = g(x(t))$. *Feedback control* takes the output $y(t)$ and feeds back a control input signal $u(t)$, which depends on y and possibly its history. In this section we discuss the case of state feedback control, $y(t) = x(t)$, to simplify notation. Feedback control needs to be designed in a way to be stabilizing and, in addition for the purposes discussed in our paper, non-invasive. Making feedback control stabilizing is a standard control theoretical task involving the construction of state observers (if necessary) and *control gains*, which are amplification factors for y entering the input u . Non-invasiveness refers to the property that the control input signal $u(t)$ vanishes in the stabilized steady states after transients have settled. When $u = 0$, up to disturbances typical for experiments, then one observes phenomena of the original uncontrolled system, where u was 0.

2.1. Design of inherently non-invasive feedback control. The most well-known example of non-invasive feedback control is time-delayed feedback [30], where $u(t) = K \cdot (x(t) - x(t-T))$. This input automatically vanishes whenever the $x(t)$ settles to an equilibrium or a periodic orbit of period T , but is not able to stabilize equilibria or periodic orbits of forced systems with single eigenvalues 0 or 1, respectively [20]. For continuation of equilibria two other classes of non-invasive control laws have been designed and investigated. First, washout filters [1, 18] add extra degrees of freedom, x_{wo} , which we formulate in the form ($x \in \mathbb{R}^{n_x}$ and $u \in \mathbb{R}^{n_u}$)

$$(2.1) \quad \dot{x}(t) = f(x(t), u(t)), \quad \dot{x}_{\text{wo}}(t) = u(t), \quad u(t) = K_{\text{st}}[x(t) - x_{\text{ref}}] + K_{\text{wo}}[x_{\text{wo}}(t) - x_{\text{wo,ref}}],$$

where $x_{\text{ref}}, x_{\text{wo,ref}}$ are constant reference values chosen by the experimenter. The feedback is non-invasive as any equilibrium of (2.1) is also an equilibrium x_{eq} of $\dot{x} = f(x, 0)$. One can find gains $(K_{\text{st}}, K_{\text{wo}})$ to make x_{eq} stable with arbitrary decay rate if and only if the matrix $\partial_1 f(x_{\text{eq}}, 0)$ is regular and the pair $(\partial_1 f(x_{\text{eq}}, 0), \partial_2 f(x_{\text{eq}}, 0))$ is controllable. Formulation (2.1)

is a generalization of the construction in the original papers [1, 18], showing that the additional degrees of freedom form the integral component of a proportional-integral (PI) control, which enforces $u = 0$ in the equilibrium. The PI control in (2.1) is degenerate, as the right-hand side for \dot{x}_{wo} depends on x only through u . This simplifies the proof of the stabilization criterion compared to the original sources [7, 18] and reduces the design of the feedback gains $(K_{\text{st}}, K_{\text{wo}})$ to a standard linear control design problem (see Lemma 3.1).

When continuing branches of equilibria, control law (2.1) fails at saddle-node (fold) bifurcations, where $\partial_1 f(x_{\text{eq}}, \mu_{\text{eq}})$ is singular, motivating a second type of non-invasive feedback law. Assuming that the dynamical system depends on a parameter $\mu \in \mathbb{R}$ and has a branch of equilibria, parameterized by a scalar, $s \mapsto (x_{\text{eq}}(s), \mu_{\text{eq}}(s))$, Siettos *et al.* [38] proposed to dynamically adjust the parameter μ using the control input u :

$$(2.2) \quad \dot{x}(t) = f(x(t), \mu(t)), \quad \dot{\mu}(t) = u(t), \quad u(t) = K_{\text{st},x}[x(t) - x_{\text{ref}}] + K_{\text{st},\mu}[\mu(t) - \mu_{\text{ref}}].$$

This feedback control law is also non-invasive in the above sense, such that one may track the branch of equilibria using pseudo-arclength continuation [2, 11, 12, 15, 24] with a sequence of points $(x_{\text{ref}}, \mu_{\text{ref}})$ predicted by the pseudo-arclength continuation algorithm. A limiting case of (2.2) was used in experiments in [6]. One can find gains $(K_{\text{st},x}, K_{\text{st},\mu})$ to make $(x_{\text{eq}}, \mu_{\text{eq}})$ stable with arbitrary decay rate if and only if the pair $(\partial_1 f(x_{\text{eq}}, \mu_{\text{eq}}), \partial_2 f(x_{\text{eq}}, \mu_{\text{eq}}))$ is controllable (see Lemma 3.2). In contrast to (2.1), control law (2.2) does not fail near saddle-node bifurcations, which are points of particular interest when performing bifurcation analysis. However, Lemma 3.2 implies that controllability through a scalar bifurcation parameter μ will break down at codimension-1 events such that one may generically encounter singularities in single-parameter continuations.

Zero-in-equilibrium feedback control. In this paper we generalize (2.1) and (2.2) to introduce a control law that avoids these singularities by combining (2.1) and (2.2). We formulate the law for the case where the ODE depends on a scalar bifurcation parameter μ and an additional scalar control input $u \in \mathbb{R}$. This permits us to introduce an additional scalar gain $a \in \mathbb{R}$ to propose the feedback

$$(2.3) \quad \dot{x}(t) = f(x(t), \mu(t), a u(t)), \quad \dot{\mu}(t) = u(t), \quad u(t) = K_{\text{st},x}[x(t) - x_{\text{ref}}] + K_{\text{st},\mu}[\mu(t) - \mu_{\text{ref}}].$$

For (2.3) one can find gains $(a, K_{\text{st},x}, K_{\text{st},\mu})$ to make $(x_{\text{eq}}, \mu_{\text{eq}})$ stable with arbitrary decay rate if and only if the matrix pair $(R_{\mu}, f_x R_u)$ is regular (polynomial $\lambda \mapsto \det(R_{\mu} + \lambda f_x R_u) \not\equiv 0$, see Lemma 3.3), where $f_x = \partial_1 f(x_{\text{eq}}, \mu_{\text{eq}}, 0)$, and R_{μ} and R_u are the controllability matrices of f_x with respect to $f_{\mu} = \partial_2 f(x_{\text{eq}}, \mu_{\text{eq}}, 0)$ and $f_u = \partial_3 f(x_{\text{eq}}, \mu_{\text{eq}}, 0)$, respectively: for $n_x = \dim x$

$$(2.4) \quad R_u = [f_u, f_x f_u, \dots, f_x^{n_x-1} f_u] \in \mathbb{R}^{n_x \times n_x}, \quad R_{\mu} = [f_{\mu}, f_x f_{\mu}, \dots, f_x^{n_x-1} f_{\mu}] \in \mathbb{R}^{n_x \times n_x}.$$

This regularity condition is violated only in events of codimension $n_x + 1$. Thus, (2.3) with suitable gains stabilizes the natural equilibria of an ODE dynamically uniformly along the whole branch for generic branches of equilibria. This is in contrast to (2.1) and (2.2), which one expects to fail at isolated points of the curve (codimension-1 events), namely when f_x is singular (for (2.1), assuming that R_u is always regular, as we can freely choose a suitable u), or when R_{μ} is singular (for (2.2)).

We use the term *zero-in-equilibrium feedback control* to indicate that the class of feedback laws (2.3) contains washout filters, (2.1), and control through parameter, (2.2), as limiting cases ($a \rightarrow \infty$ and $a = 0$), but is less general than “non-invasive” which includes time-delayed feedback.

Figure 3.1 in section 3 shows a sketch how control through the bifurcation parameter, (2.2) and zero-in-equilibrium control (2.3) affect the flow near the equilibrium branch in the case of scalar x .

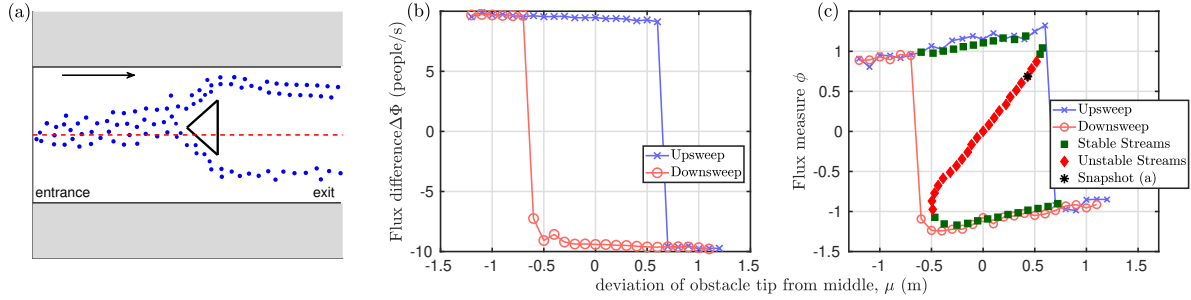


Figure 2.1. Response of a flow of $N = 100$ pedestrians through a corridor to an obstacle, depending on the obstacle position μ , relative to middle of corridor. (a) Top view snapshot of pedestrians (blue dots) moving through a $20\text{ m} \times 10\text{ m}$ corridor past an obstacle. (b) Parameter sweep, changing distance μ of obstacle tip from red dashed line in Figure 2.1(a), and response $\Delta\Phi$, given in (4.6). The coordinates of the snapshot Figure 2.1(a) are indicated as a star symbol in Figure 2.1(c). (c) Full bifurcation diagram obtained using the newly proposed control law (2.3) and the spatially averaged flux measure ϕ , given in (4.7).

2.2. Demonstration on multi-particle model for pedestrian flow. To illustrate continuation with non-invasive feedback control, we consider a particle model describing pedestrians moving through a corridor past an obstacle in an evacuation scenario.

The microscopic behavior of every pedestrian (treated as a point particle) is based on the social force model by Helbing and Molnar [19] with an additional preference of pedestrians toward alignment with near-by others moving in roughly the same direction [40]. All pedestrians are moving towards the end of the corridor, as shown in Figure 2.1(a). Inside the corridor there is a triangular obstacle which blocks the pedestrians’ straight path to the exit. As a result, they have to choose a route, left or right of the obstacle from their point of view (see top view Figure 2.1(a)). The position μ of the obstacle relative to the middle of the corridor (vertical distance of triangle tip from red dashed line in Figure 2.1(a)) changes the pedestrians’ preference for each route. We consider this position (measured in meters) as the system parameter μ . The macroscopic variable of interest is the difference between the flows of pedestrians along the two different routes. Figure 2.1(b) shows the time-averaged flux difference $\Delta\Phi$, given in (4.6), between left and right route, measured in people per second.

This particle system exhibits a bistability and hysteresis phenomenon: once the majority of pedestrians has chosen a particular route, even a small alignment effect will cause pedestrians to follow the flow, even if the current route is less direct than the alternative, until there is a sudden transition of the pedestrian flow to the other route. Figure 2.1(b) shows this effect in a parameter study for obstacle position μ , where the obstacle is gradually shifted, first from

$\mu = -1.25$ m upwards to 1.25 m (in blue, with crosses), then downwards again (in red, with circles). There is a large region of bistability, which leads to the hypothesis that the sudden transitions at macroscopic level are saddle-node bifurcations, and that there is a branch of unstable steady flows inside this bistability region, which acts as a threshold for disturbances to cause spontaneous transition.

Control-based continuation using control law (2.3) confirms this hypothesis for the particle model as shown in Figure 2.1(c). Here the y -axis is a spatially averaged flux difference ϕ , which the feedback control input u depends on (see (4.7) and Figure 4.3b for definition of ϕ). The control-based continuation enables us to produce the full bifurcation diagram, including both stable and unstable steady flows, without the need of having access to any effective macroscopic model. Control law (2.3) turns out to be especially advantageous compared to parameter control (2.2) (which would in principle also be feasible) because we are free to choose the control input u without additional computational cost. In laboratory experiments additional inputs may require additional actuation equipment. We choose a bias force acting on pedestrians directly in front of the obstacle (see (4.9) and Figure 4.3a for definition of input). The modulus of u is always small when controlling perturbations (due to random entry of the pedestrians into the corridor) with this bias force, while (2.2) caused large corrections in $\mu(t)$.

3. Equation-free bifurcation analysis and control-based continuation. Various methods have been proposed to avoid the need for an explicit macroscopic model for the bifurcation analysis required for high-level qualitative analysis. Equation-free methods pioneered by Kevrekidis *et al.* [21, 22] have been applied primarily to computational experiments originating from multi-particle simulations, while methods based on feedback control were developed for physical experiments [30, 43, 4].

This section reviews the two fundamentally different methods briefly. We then show how unifying the known inherently non-invasive feedback control for equilibria of nonlinear systems laws as special cases of control with an integral component allows us to design control law (2.3), which does not suffer from singularities one would encounter along a generic branch of equilibria. This makes (2.3) applicable to the particle flow simulation of a pedestrian evacuation scenario such that we can perform control-based continuation using inherently non-invasive feedback control, without requiring numerical root-finding algorithms. Continuation using (2.3) also does not rely on information about partial derivatives at every step.

One conclusion from our paper is that feedback control-based methods may also be an easy-to-implement approach to equation-free analysis in computational experiments.

3.1. Equation-free analysis based on lift-evolve-restrict cycles. The methodology originally proposed by Kevrekidis *et al.* (see e.g., [21, 22] for reviews), named *equation-free analysis*, is able to perform high-level tasks, such as bifurcation analysis or optimization of macroscopic behavior, on complex simulations (such as multi-particle models) by judiciously initialized simulations, without explicitly deriving a macroscopic model. This is done by extracting numerical information about the macroscopic behavior using suitable short simulation bursts of the microscopic model as part of a *lift-evolve-restrict* loop. The basic method requires the user to specify a projection of the microscopic state into the space of macroscopic quantities of suitable dimension (the restriction operator), and an embedding of the (low-dimensional) macroscopic state space into the state space of the microscopic complex simulation (the lifting

operator). With the use of data analysis techniques such as diffusion maps it may be possible to determine the dimension and numerically optimal restriction projection for the macroscopic variables automatically [9, 10, 39]. Equation-free analysis assumes that the *lifting* operator maps close to an assumed-to-exist attracting slow manifold, on which the macroscopic evolution takes place. To compensate for the error of not lifting exactly on this manifold, an implicit formulation of the lifting operator can be used [26, 36, 42].

Equation-free analysis based on lift-evolve-restrict cycles has also been applied to agent-based models such as epidemic networks by Gross and Kevrekidis [17] and a population of traders participating in a financial market by Siettos *et al.* [37] and Tsoumanis and Siettos [41]. The analysis in [37] concluded by applying a washout filter similar to (2.1) to make an unstable steady state visible in simulations without lifting, while [41] applied systematic corrections to the bifurcation parameter similar to (2.2).

3.2. Control-based continuation. Mechanical engineering and physics research into discovering dynamically unstable phenomena in physical experiments with nonlinear behavior took a different approach to equation-free analysis, which is more suitable to physical experiments [4, 30, 35, 43] as most experiments cannot be initialized at arbitrary points in state space.

3.2.1. Existence of underlying ODE and equilibria. Control-based continuation assumes that the underlying dynamical system (which will be a stochastic multi-particle model in our case) is governed by a system of ordinary differential equations with a state $x(t)$ depending on a scalar parameter μ , and with control inputs $u(t)$ and outputs $y(t) = g(x(t))$. This approach also makes assumptions concerning existence of equilibria, and controllability and observability near these equilibria as listed below.

In order to perform control-based continuation to an experiment, the control is applied with the feedback laws designed based on the aforementioned assumptions. Then one validates during the experiments whether the feedback controlled system converges to an equilibrium to a sufficiently good approximation given by the tolerances of the experimental measurement equipment and expected disturbances.

Equivalently, when applying these experimental techniques to a dynamical system given in the form of a simulation (such as our particle model for pedestrians), then the simulation is treated like a computational experiment. For systems with a large number N of interacting particles one may repeat the computational experiment with different N to observe whether a law of large numbers holds, such that one has convergence of the feedback controlled system to an equilibrium for increasing N .

Assumption 3.1 (Equilibrium branch for system of ODEs). *The dynamical system is assumed to be governed by a system of ODEs of the form*

$$(3.1) \quad \dot{x}(t) = f(x(t), \mu, u(t)), \quad \text{where } f : \mathbb{R}^{n_x} \times \mathbb{R} \times \mathbb{R}^{n_u} \rightarrow \mathbb{R}^{n_x}.$$

We assume that for $u(t) = 0$, (3.1) has an isolated branch (curve) of equilibria, parameterized by $s \in [s_{\min}, s_{\max}] \subset \mathbb{R}$, $(x_{\text{eq}}(s), \mu_{\text{eq}}(s))$, satisfying $0 = f(x_{\text{eq}}(s), \mu_{\text{eq}}(s), 0) = 0$ for all $s \in [s_{\min}, s_{\max}]$.

Initially we will discuss state feedback control, where we assume that the control input u

may depend on all components of the state $x(t) \in \mathbb{R}^{n_x}$. The for physical experiments more realistic case of output feedback control, where only some output $y = g(x(t))$ may enter the algebraic or dynamic rule for u will be briefly discussed afterwards. The general criteria for non-invasiveness are identical for output feedback to those of state feedback control. We will consider output feedback in detail for the concrete criteria for choosing feedback gains in [Subsection 3.4](#). In a computational experiment the full state is available, and one typically chooses a few problem-specific quantities that enter the control input. [Figure 2.1](#) showed two different flux measures, $\Delta\Phi$ and ϕ , as possible outputs.

3.2.2. Controllability. We abbreviate the partial derivatives of f in the equilibria by

$$\begin{aligned} f_x &:= \partial_1 f(x_{\text{eq}}, \mu_{\text{eq}}, 0) \in \mathbb{R}^{n_x \times n_x}, & f_\mu &:= \partial_2 f(x_{\text{eq}}, \mu_{\text{eq}}, 0) \in \mathbb{R}^{n_x \times 1}, \\ f_u &:= \partial_3 f(x_{\text{eq}}, \mu_{\text{eq}}, 0) \in \mathbb{R}^{n_x \times n_u} \end{aligned}$$

(dropping the argument s in all expressions here). We recall that a linear constant-coefficient system $\dot{x} = Ax + Bu$ with matrices $A \in \mathbb{R}^{n_x \times n_x}$ and $B \in \mathbb{R}^{n_x \times n_u}$ is controllable if the matrix $[B, AB, \dots, A^{n_x-1}B]$ has full rank n_x (for standard textbooks on control theory and controllability see [\[3, 13\]](#)). Controllability implies that there exist *feedback gains* $K_{\text{cn}} \in \mathbb{R}^{n_u \times n_x}$ such that $A + BK_{\text{cn}}$ is a Hurwitz matrix. More precisely, the spectrum of $A + BK_{\text{cn}}$ can be placed arbitrarily by suitable choice of K_{cn} .

The above statements on classical controllability imply in particular that generically a single input ($n_u = 1$) can be used to stabilize the equilibrium $(x_{\text{eq}}(s), \mu_{\text{eq}}(s))$ for any fixed s (no matter how many unstable directions $n_{\text{unst}}(s)$ it has with $u = 0$) locally, by the scalar state feedback

$$(3.2) \quad u = K_{\text{cn}} \cdot (x - x_{\text{eq}}).$$

The local exponential decay rate toward x_{eq} can be made arbitrarily large with suitably chosen gains. In practice, stability becomes sensitive with respect to the gains if one attempts to stabilize many unstable degrees of freedom. Since the stabilizing gains depend on the partial derivatives f_x, f_u one needs good estimates for these. As we consider scenarios where we do not have accurate estimates for partial derivatives, we will in [Subsection 3.4](#) construct simple criteria for the gains in the single-input single-output case $n_u = 1$ and one degree of instability or less ($n_{\text{unst}} \leq 1$).

3.2.3. Non-invasiveness. As the concept of controllability recalled above is about linear systems, when applying it to the vicinity of equilibria in nonlinear systems one has to assume that the equilibrium location and the partial derivatives f_x and f_u are known. Observe that [\(3.2\)](#) contains x_{eq} in its construction. In practice, one constructs the feedback gains K_{cn} from estimates \hat{f}_x and \hat{f}_u , and inserts a *reference value* x_{ref} into [\(3.2\)](#):

$$(3.3) \quad u = K_{\text{cn}} \cdot (x - x_{\text{ref}}).$$

If the perturbations $\hat{f}_x - f_x, \hat{f}_u - f_u$ and $x_{\text{ref}} - x_{\text{eq}}$ are sufficiently small then the feedback gains K_{cn} constructed for \hat{f}_x and \hat{f}_u are stabilizing the equilibrium. That is, the controlled system [\(3.1\)](#), [\(3.3\)](#) will have an equilibrium x_{cn} near x_{eq} . Importantly,

$$(3.4) \quad x_{\text{cn}} = x_{\text{eq}} + O(x_{\text{ref}} - x_{\text{eq}}).$$

That is, if $x_{\text{ref}} = x_{\text{eq}}$ then small perturbation in the partial derivatives $\hat{f}_x - f_x$ and $\hat{f}_u - f_u$ will not change the location of the equilibrium of the controlled system.

The application of feedback control to discover the precise equilibria (or, more generally, steady states including periodic orbits) motivates the concept of non-invasiveness. When does it hold that $x_{\text{cn}} = x_{\text{eq}}$? Or, in other words, how to control the system such that the observed equilibrium coincides with the unknown equilibrium of the uncontrolled system?

3.2.4. Non-invasiveness through iterative root finding. If we assume controllability for all s along the branch, and we assume that the gain $K_{\text{cn}}(s) \in \mathbb{R}^{1 \times n_x}$ depends smoothly on s (for example, if it is constant), then the locally stabilizing feedback control (3.3), $u(t) = K_{\text{cn}}[x(t) - x_{\text{ref}}]$, for $x_{\text{ref}} \approx x_{\text{eq}}(s)$ induces the input-output map

$$(3.5) \quad X_{\infty} : \mathbb{R}^{n_x} \times \mathbb{R} \ni (x_{\text{ref}}, \mu) \mapsto x_{\text{cn}} = \lim_{t \rightarrow \infty} x(t) \in \mathbb{R}^{n_x}.$$

This map X_{∞} is evaluated at an argument (x_0, μ_0) near the branch $(x_{\text{eq}}(s), \mu_{\text{eq}}(s))$ by setting the reference value $x_{\text{ref}} = x_0$ in (3.3), the parameter $\mu = \mu_0$ in the system, (3.1), waiting for the transient dynamics of (3.1) to settle such that the state $x(t)$ reaches a limit x_{cn} . By construction, the branch of equilibria $(x_{\text{eq}}(s), \mu_{\text{eq}}(s))$ are fixed points of the map X_{∞} , that is, they are solutions of the equation

$$(3.6) \quad X_{\infty}(x, \mu) = x$$

for all $s \in [s_{\text{min}}, s_{\text{max}}]$: when state $x(t)$ equals x_{ref} in (3.3) then $u = 0$ such that the feedback control is non-invasive.

The papers [35, 5, 8, 4] tracked branches of forced oscillations directly in mechanical vibration experiments by applying linear feedback control (typically proportional-plus-derivative feedback control) to the forced nonlinear oscillators, and then used standard numerical root-finding algorithms, such as simplified Newton iterations, to find root curves of fixed point problem (3.6).

As implementing a stabilizing feedback loop is often the most difficult part in physical experiments, permitting the experimenter to choose gains with as few restrictions as possible is important [4]. The study [8] performs a systematic investigation on how the gains can be chosen but other experimental papers keep them constant along the branch. Using maps X_{∞} where u is based on adaptive feedback gains is possible and improves robustness to uncertainty and time delays [25]. Its effect has been demonstrated on ODEs similar to (3.1).

A major obstacle for the application of standard root-finding algorithms to solving (3.6) is that experimentally obtained data has high uncertainty such that precise derivative information for the Jacobian of X_{∞} is not available or expensive to obtain, especially in higher dimensions. This may lead to slow and uncertain convergence, negating the main advantage of classical numerical local root-finding and continuation algorithms such as Newton iterations and pseudo-arclength continuation. Schilder *et al.* [34] developed and studied modifications of these classical numerical methods, specifically to treat contamination with noise, which are now available as CONTINEX toolbox in COCO [11].

3.3. Inherently non-invasive feedback control. When the idea of finding unstable steady states (including periodic orbits) by continuous-time feedback control was originally conceived,

the focus was on types of feedback that are inherently non-invasive. These feedback laws introduce additional degrees of freedom x_{wo} . We will show that, in a suitable formulation, these additional degrees of freedom act like integral components of a proportional-plus-integral (PI) control, enforcing an additional constraint, which is in this case $u = 0$. With this formulation, it becomes clear how to generalize existing types of inherently non-invasive feedback to remove singularities at special points.

3.3.1. Inherently non-invasive control — washout filters. For equilibria, the additional variables x_{wo} have been introduced by [31, 43] in the form of state observers and were called washout filter in [43] (hence the subscript wo). Let us repeat the full non-linear ODE such that the feature of non-invasiveness becomes clear (we keep s and, thus, μ fixed):

$$(3.7) \quad \dot{x} = f(x, \mu, u), \quad \dot{x}_{\text{wo}} = u, \quad \text{where } x_{\text{wo}} \in \mathbb{R}^{n_u}.$$

The differential equation for x_{wo} implies that, whenever a linear feedback law of the general form

$$(3.8) \quad u(t) = k_{\text{st}} \cdot (x - x_{\text{ref}}) + k_{\text{wo}} \cdot (x_{\text{wo}} - x_{\text{wo,ref}}) \text{ with arbitrary } k_{\text{st}} \in \mathbb{R}^{n_u \times n_x} \text{ and } k_{\text{wo}} \in \mathbb{R}^{n_u \times n_u}$$

is applied, every equilibrium of (3.7), (3.8) has $u = 0$. Thus, equilibria of (3.7), (3.8) have a x -component that is also an equilibrium of the uncontrolled system $\dot{x} = f(x, \mu, 0)$ such that (3.7), (3.8) does not change the locations of equilibria of the uncontrolled system. This justifies the notion of inherent non-invasiveness for this type of feedback control. A simple criterion, given in Lemma 3.1, shows that a system is controllable with washout filters whenever we have linear state feedback controllability along the equilibrium branch $(x_{\text{eq}}(s), \mu_{\text{eq}}(s))$, except when f_x is singular.

Lemma 3.1 (Controllability for washout filters). *The linear time-invariant (autonomous) system*

$$(3.9) \quad \dot{x} = Ax + Bu, \quad \dot{x}_{\text{wo}} = u \quad \text{with } A \in \mathbb{R}^{n_x \times n_x}, B \in \mathbb{R}^{n_x \times n_u},$$

is controllable if and only if $\dot{x} = Ax + Bu$ is controllable and A is regular.

Proof of Lemma 3.1. The coefficients for the state $x_{\text{ext}} = (x, x_{\text{wo}})$ and control u in the right-hand side in (3.9) have the form (I is the identity matrix)

$$A_{\text{ext}} = \begin{bmatrix} A & 0 \\ 0 & 0 \end{bmatrix}, \quad B_{\text{ext}} = \begin{bmatrix} B \\ I_{n_u \times n_u} \end{bmatrix}.$$

Thus, the controllability matrix R_{ext} of the extended system has the form

$$R_{\text{ext}} = \begin{bmatrix} B & AB & \cdots & A^{n_x+n_u-1}B \\ I_{n_u \times n_u} & 0 & \cdots & 0 \end{bmatrix},$$

which has rank $n_x + n_u$ if and only if the matrix $[AB, \dots, A^{n_x}B] = A[B, AB, \dots, A^{n_x-1}B]$ has rank n_x , where $[B, AB, \dots, A^{n_x-1}B]$ is the controllability matrix of $\dot{x} = Ax + Bu$. \square

Formulation (3.7), (3.8) is different from the original papers [1, 18, 43]. Let us briefly explain that (3.7), (3.8) encompasses the original washout filter formulations. The most general version for continuous-time washout filters introduced by Hassouneh *et al.* [18] is of the form (dropping nonlinear terms)

$$(3.10) \quad \dot{x} = Ax + Bu, \quad \dot{z} = P(x - z), \quad u = K(x - z)$$

with non-singular $P \in \mathbb{R}^{n_x \times n_x}$ and $z \in \mathbb{R}^{n_x}$. The authors showed that when the pair (A, B) is stabilizable and A is non-singular then one can find P, K such that (3.10) is asymptotically stable. System (3.10) is a special case of (3.9) with a particular choice of gains if we assume that the gain K in (3.10) is a full-rank $n_u \times n_x$ matrix and that $n_u \leq n_x$. To see this, let us call $B_{\text{ext}} = [B, 0_{n_x \times (n_u - n_x)}]$ and choose a matrix $\tilde{K} \in \mathbb{R}^{(n_x - n_u) \times n_x}$ such that $[K^\top, \tilde{K}^\top]$ is non-singular. Then the variable

$$\begin{bmatrix} y \\ \tilde{y} \end{bmatrix} = \begin{bmatrix} K \\ \tilde{K} \end{bmatrix} P^{-1} z$$

and x satisfy

$$(3.11) \quad \dot{x} = Ax + B_{\text{ext}} \begin{bmatrix} u \\ \tilde{u} \end{bmatrix}, \quad \begin{bmatrix} \dot{y} \\ \dot{\tilde{y}} \end{bmatrix} = \begin{bmatrix} u \\ \tilde{u} \end{bmatrix}$$

if x and z satisfy system (3.10). System (3.11) is of the same form as our formulation (3.9) of the washout filter in Lemma 3.1, with $n_x - n_u$ components of the control input unused. The form of system (3.10) corresponds then to the particular choice of gains

$$k_{\text{st}} = \begin{bmatrix} K \\ \tilde{K} \end{bmatrix}, \quad k_{\text{wo}} = \begin{bmatrix} K \\ \tilde{K} \end{bmatrix} P \begin{bmatrix} K \\ \tilde{K} \end{bmatrix}^{-1}$$

in our formulation (3.7), (3.8). Thus, Lemma 3.1 extends and simplifies the results of [7, 18], as our result immediately implies all conclusions from controllability of linear systems with constant coefficients. It also separates the problem of controllability from the problem of finding the control gains, which can then be designed using standard linear feedback control theory.

3.3.2. Inherently non-invasive feedback control through the parameter. Siettos *et al.* [38] showed that, if state feedback control is applied through the bifurcation parameter μ , then an inherently non-invasive control can be constructed in the context of a continuation of a branch of equilibria in μ . The feedback control in [38] considers μ as part of the state, satisfying the equation

$$(3.12) \quad \dot{\mu}(t) = 0 + u(t).$$

In the setting of [38] this is the only point where control input u enters, such that this method considers a scalar control input, $n_u = 1$, for one-parameter equilibrium branches. Thus, (3.1) has the form

$$(3.13) \quad \dot{x}(t) = f(x(t), \mu(t)).$$

Siettos *et al.* observe that state feedback control of system (3.12), (3.13) of the form

$$(3.14) \quad u(t) = K_{st,x}(x(t) - x_{\text{ref}}) + K_{st,\mu}(\mu(t) - \mu_{\text{ref}})$$

is always non-invasive in the sense that equilibria of the controlled system must satisfy $u = 0$, such that they will lie on the intersection of the equilibrium curve $(x_{\text{eq}}(\cdot), \mu_{\text{eq}}(\cdot))$ with the codimension-1 hyperplane $u = 0$ in the (x, μ) -space. Siettos *et al.* [38] demonstrated continuation through their feedback control for a kinetic Monte-Carlo simulation. A control law similar to (3.14) was proposed for Poincare maps of periodic orbits in [27]. Physical experiments on vibrations of nonlinear mechanical oscillators were performed by [6] on a further simplification of (3.12), (3.13), (3.14) by applying the feedback control law

$$(3.15) \quad \mu(t) = \mu_{\text{ref}} + K_{st} \cdot (x(t) - x_{\text{ref}}),$$

which corresponds to choosing $|K_{st,\mu}|, |K_{st,x}| \gg 1$ with fixed ratio $K_{st} = K_{st,x}/K_{st,\mu}$ in (3.14). This law is also non-invasive whenever it is stabilizing.

Lemma 3.2 (Controllability for parameter control).

An equilibrium $(x_{\text{eq}}(s), \mu_{\text{eq}}(s))$ of (3.12), (3.13) is controllable if and only if the pair of partial derivatives $(f_x(s), f_\mu(s))$ in $(x_{\text{eq}}(s), \mu_{\text{eq}}(s))$ is controllable.

Proof of Lemma 3.2. The coefficients for the state $x_{\text{ext}} = (x, \mu)$ and control u in the right-hand side in (3.12), (3.13) have the form

$$A_{\text{ext}} = \begin{bmatrix} f_x & f_\mu \\ 0 & 0 \end{bmatrix}, \quad B_{\text{ext}} = \begin{bmatrix} 0 \\ 1 \end{bmatrix}.$$

Thus, the controllability matrix R_{ext} of the extended system has the form

$$R_{\text{ext}} = \begin{bmatrix} 0 & f_\mu & f_x f_\mu & \cdots & f_x^{n_x-1} f_\mu \\ 1 & 0 & 0 & \cdots & 0 \end{bmatrix}.$$

This matrix has rank $n_x + 1$ if and only if the matrix $[f_\mu, \dots, f_x^{n_x-1} f_\mu]$ has rank n_x , which is the controllability matrix of the system $\dot{x} = f_x x + f_\mu u$. \square

Thus, the controllability condition for (3.14) is the same as for the simplified control law (3.15).

3.3.3. Inherently non-invasive control – zero-in-equilibrium feedback. Both methods for inherently non-invasive control of equilibria are expected to fail at isolated points along the one-parameter equilibrium branch $(x_{\text{eq}}(s), \mu_{\text{eq}}(s))$ for

$$(3.16) \quad \dot{x} = f(x, \mu, u).$$

For controllability through the inputs μ or u on their own, the relevant controllability matrices are (dropping argument s)

$$(3.17) \quad R_u = [f_u, f_x f_u, \dots, f_x^{n_x-1} f_u] \in \mathbb{R}^{n_x \times (n_x \cdot n_u)},$$

$$(3.18) \quad R_\mu = [f_\mu, f_x f_\mu, \dots, f_x^{n_x-1} f_\mu] \in \mathbb{R}^{n_x \times n_x}.$$

- **Failure at singular $f_x(s)$:** Washout filter based control with input u for (3.16) do not stabilize the equilibrium near fold bifurcations. This failure occurs even if the pair $(f_x(s), f_u(s))$ is controllable in the parameter s of the fold bifurcation, that is, when $R_u(s)$ has rank n_x .
- **Failure at singular $R_\mu(s)$:** For one-parameter branches the control input for parameter control is naturally one-dimensional ($n_u = 1$) such that a loss of controllability (singularity of $R_\mu(s)$) is a codimension-1 event, expected to occur at isolated points along the branch $(x_{\text{eq}}(s), \mu_{\text{eq}}(s))$.

In the particle flow model example in Section 4 the time scale of the response of the particle flow to parameter changes (in our case the position μ of the obstacle) is also too slow, such that non-invasive feedback control, when applied purely through the bifurcation parameter, creates a large uncertainty in the resulting steady states x_{eq} , observed as limits $\lim_{t \rightarrow \infty} x(t)$ after transients have settled. See also Section 5 where we briefly discuss control through the bifurcation parameter.

Hence, we extend feedback control with washout filters by using the bifurcation parameter μ as the integral component, in the same way as in the feedback control through the parameter. This permits us to design an inherently non-invasive control that is only singular at events of codimension larger or equal than 2. Let us consider the feedback control scheme

$$(3.19) \quad \dot{x} = f(x, \mu, au), \quad \dot{\mu} = u \quad \text{with } \dim u = 1 \text{ (thus, } n_u = 1), \text{ and } a \in \mathbb{R},$$

such that u is an input in f in addition to the also adjustable μ . The scalar a acts as an additional weight on the control gains in f compared to $\dot{\mu}$, which we are free to choose suitably. We observe that this feedback is also inherently non-invasive: every equilibrium of (3.19) is also an equilibrium of the uncontrolled system (3.16) with $u = 0$. We refer to (3.19) as *zero-in-equilibrium feedback control*.

Lemma 3.3 (Controllability for zero-in-equilibrium feedback control).

The equilibrium $(x_{\text{eq}}, \mu_{\text{eq}})$ of (3.19) is controllable if the matrix $af_x R_u + R_\mu$ is regular, where R_u and R_μ are the controllability matrices defined in (3.17) and (3.18).

Proof of Lemma 3.3. The coefficients of the linearization of system (3.19) are

$$A_{\text{ext}} = \begin{bmatrix} f_x & f_\mu \\ 0 & 0 \end{bmatrix}, \quad B_{\text{ext}} = \begin{bmatrix} af_u \\ 1 \end{bmatrix}.$$

Thus, the controllability matrix for the linearized system is

$$R_{\text{ext}} = \begin{bmatrix} af_u & af_x f_u + f_\mu & af_x^2 f_u + f_x f_\mu & \dots & af_x^{n_x} f_u + f_x^{n_x-1} f_\mu \\ 1 & 0 & 0 & \dots & 0 \end{bmatrix},$$

which has rank $n_x + 1$ if and only if $af_x \cdot R_u + R_\mu$ is regular. \square

When constructing non-invasive control, one faces the question when one can find a scalar a for which the equilibrium $(x_{\text{eq}}, \mu_{\text{eq}})$ is controllable. We may phrase the answer given by Lemma 3.3 in terms of regularity of the matrix pair $(R_\mu, f_x R_u)$ of $\mathbb{R}^{n_x \times n_x}$ matrices. A pair (A_0, A_1) of $\mathbb{R}^{n_x \times n_x}$ matrices is called regular, if the polynomial $\lambda \mapsto \det(A_0 + \lambda A_1)$ is not identically zero. The condition on the coefficients in the two matrices A_0 and A_1 for the pair

to be singular (i.e., not regular) imposes $n_x + 1$ constraints: all coefficients of the characteristic polynomial $\lambda \mapsto \det(A_0 + \lambda A_1)$ have to be zero. Thus, violations of matrix pair regularity are codimension $n_x + 1$ events. [Corollary 3.4](#) summarizes the consequences of linear feedback controllability for control law [\(3.19\)](#).

Corollary 3.4 (Existence of stabilizing gains). *Let $\gamma > 0$ be arbitrary. If the matrix pair $(R_\mu, f_x R_u)$ is regular for the linearization of $\dot{x} = f(x, \mu, 0)$ in equilibrium $(x_{\text{eq}}, \mu_{\text{eq}})$, then there exist control gains $K_{\text{st},x} \in \mathbb{R}^{1 \times n_x}$, $K_{\text{st},\mu} \in \mathbb{R}$, $a \in \mathbb{R}$, such that the controlled system $\dot{x} = f(x, \mu, au)$, $\dot{\mu} = u$ with*

$$(3.20) \quad u = K_{\text{st},x}(x_{\text{ref}} - x) + K_{\text{st},\mu}(\mu_{\text{ref}} - \mu)$$

has for all $(x_{\text{ref}}, \mu_{\text{ref}}) \approx (x_{\text{eq}}, \mu_{\text{eq}})$ a stable equilibrium $(x_{\text{cn}}, \mu_{\text{cn}}) \approx (x_{\text{eq}}, \mu_{\text{eq}})$, which is reached with local exponential decay rate greater than γ .

Proof of Corollary 3.4. We choose the weight a such that $af_x R_u + R_u$ is regular, which is possible by the regularity of the matrix pair. The resulting controllability of the linearization in $(x_{\text{eq}}, \mu_{\text{eq}})$ permits us to choose gains $(K_{\text{st},x}, K_{\text{st},\mu})$ such that the linearization of system [\(3.19\)](#) in $(x_{\text{eq}}, \mu_{\text{eq}})$ with feedback control u given in [\(3.20\)](#) and $(x_{\text{ref}}, \mu_{\text{ref}}) = (x_{\text{eq}}, \mu_{\text{eq}})$ has a spectrum where all eigenvalues have real part less than $-\gamma$. Continuity then ensures that the decay rates and the equilibrium persist for $(x_{\text{ref}}, \mu_{\text{ref}})$ near $(x_{\text{eq}}, \mu_{\text{eq}})$. \square

In contrast to the washout filters [\(3.7\)](#) or control through the bifurcation parameter [\(3.13\)](#), [\(3.14\)](#), for which controllability conditions fail at events of codimension 1, control law [\(3.19\)](#), using the bifurcation parameter as observer and an additional control input u , fails only at events of codimension $n_x + 1$.

Adding a real-time feedback control input u imposes a cost in physical experiments. However, in computational experiments such as our particle flow model for a pedestrian evacuation scenario, an additional input has negligible cost and can be constructed to make choosing stabilizing gains $(a, K_{\text{st},x}, K_{\text{st},\mu})$ as easy as possible.

3.4. Branches with single slow dimension. The statements in [Subsection 3.3](#) are concerned with non-invasive controllability of systems with arbitrary state dimension n_x . In particular, they permit an arbitrary number n_{unst} of unstable dimensions for the equilibrium $(x_{\text{eq}}, \mu_{\text{eq}})$. General control theory also gives explicit procedures to construct gains (such as $(K_{\text{st},x}, K_{\text{st},\mu})$ in [\(3.14\)](#) or [\(3.20\)](#)) resulting in arbitrary decay rates toward the controlled equilibrium. However, these procedures rely on precise knowledge of the partial derivatives f_x and f_u , and the results are sensitive to errors in estimating these derivatives. For this reason we now discuss the common scenario that $n_{\text{unst}} \leq 2$ and that f_x , f_μ , f_u or g_x are difficult or computationally expensive to approximate. For these cases we can state simple inequality constraints on the scalar gains that ensure stabilization.

In particular we hypothesized that two fold bifurcations and a branch of unstable equilibria cause the bistability in our multi-particle model for pedestrians, shown in [Figure 2.1](#). This implicitly includes the hypothesis that the model behaves essentially as a system of ODEs close to a branch of equilibria where the number of dimensions changing stability equals 1, and where all other eigenvalues in the equilibria have uniformly negative real part. The fluctuations observed around a stable stationary particle flow are then treated as perturbations generating uncertainty, similar to a physical experiment.

For this case of an essentially one-dimensional ODE the criteria for gains in the non-invasive control schemes discussed in [Subsection 3.2](#) and [Subsection 3.3.3](#) to achieve at least stabilization can be simplified and made explicit, which we will discuss in this section.

We consider the system with output

$$(3.21) \quad \dot{x} = f(x, \mu, u), \quad y = g(x) \quad \text{with } n_y = \dim y = n_u = \dim u = 1$$

for the case where along the branch of equilibria $(x_{\text{eq}}(s), \mu_{\text{eq}}(s))$ the Jacobian $f_x(s)$ has only one direction $v_c(s)$ in which the growth rate $\lambda_c(s)$ is of order 1, while all other directions are strongly stable with time scale difference of order ϵ . More precisely:

Assumption 3.2 (Time scale difference and single slow (center) direction). *We assume that the Jacobian $f_x(s)$ in the equilibrium $(x_{\text{eq}}(s), \mu_{\text{eq}}(s))$ of (3.21) with $u = 0$ has a single simple eigenvalue $\lambda_c(s) \in \mathbb{R}$ with right and left eigenvectors $v_c(s)$, $w_c(s) \in \mathbb{R}^{n \times 1}$ with modulus of order $O(1)$, while all others are stable with time scale ratio ϵ :*

$$(3.22) \quad f_x v_c = \lambda_c v_c, \quad w_c^\top f_x = \lambda_c w_c^\top \quad \text{with scaling } 1 = w_c^\top v_c, \quad |\lambda_c| = O(1), \quad \text{and}$$

$$(3.23) \quad \text{Re} \left[\text{spec } f_x|_{\ker w_c^\top} \right] < -c_{\text{spec}}/\epsilon \quad \text{and} \quad \left\| \left[f_x|_{\ker w_c^\top} \right]^{-1} \right\| \leq \epsilon c_{\text{st}}$$

for some positive constants c_{spec} and c_{st} of order 1 and $\epsilon \ll 1$.

All variables in [Assumption 3.2](#), λ_c , v_c , w_c and $f_x|_{\ker w_c^\top}$, depend on s but c_{st} , c_{spec} and ϵ are independent of s . In (3.23) $f_x(s)|_{\ker w_c^\top}$ is the stable part of the Jacobian $f_x(s)$.

Assumption 3.3 (Partial linear observability of slow direction). *We assume that for all $s \in [s_{\text{min}}, s_{\text{max}}]$*

$$(3.24) \quad \mathbb{R} \ni g_x(s)v_c(s) \neq 0 \quad (\text{partial observability}).$$

Thus, the scalar quantity $g_x(s)v_c(s)$ never changes sign along the branch and we may scale the eigenvector $v_c(s)$ such that

$$(3.25) \quad 1 = g_x(s)v_c(s) \quad \text{for all } s \in [s_{\text{min}}, s_{\text{max}}].$$

Assumption (3.24) is a weaker genericity assumption than full linear observability, as we only want to observe the slow direction v_c through output $y = g(x)$. In contrast, assumptions such as

$$(3.26) \quad \mathbb{R} \ni w_c^\top(s)f_u(s) \neq 0 \quad (\text{partial controllability through } u), \quad \text{or}$$

$$(3.27) \quad \mathbb{R} \ni w_c^\top(s)f_\mu(s) \neq 0 \quad (\text{partial controllability through } \mu),$$

are not necessarily weaker genericity assumptions than the respective full controllability, as we do not want to rely on the coupling from stable directions in $\ker w_c^\top$ for stabilizing the equilibrium in the v_c direction. So, we are not making controllability assumptions at this stage but will consider them later for each particular type of non-invasive control laws.

In the ϵ -vicinity of an equilibrium $(x_{\text{eq}}(s), \mu_{\text{eq}}(s))$ we split the deviation of the state $x(t)$ from its equilibrium into its slow and its stable parts,

$$(3.28) \quad x_{\text{dev}}(t) := x(t) - x_{\text{eq}}(s) = v_c(s)x_c(t) + V_{\text{stb}}(s)x_{\text{stb}}(t).$$

(dropping the argument s from the deviation) where the rows of $V_{\text{stb}}(s) \in \mathbb{R}^{n \times (n-1)}$ span $\ker w_c^\top(s)$ (i.e., $0 = w_c^\top(s)V_{\text{stb}}(s)$, $I = V_{\text{stb}}^\top(s)V_{\text{stb}}(s) \in \mathbb{R}^{(n-1) \times (n-1)}$) and $x_c(t) \in \mathbb{R}$, $x_{\text{stb}} \in \mathbb{R}^{n-1}$ with $|x_c|, \|x_{\text{stb}}\| = O(\epsilon)$.

The different non-invasive control laws, discussed in [Subsection 3.3](#), applied to system [\(3.21\)](#) with scalar output and single slow dimension ([Assumption 3.2](#)) result in the expressions and conditions for control gains, discussed in the following paragraphs.

3.4.1. Non-invasive control based on washout filters. The general principle was discussed in [Subsection 3.3.1](#). For partial controllability through input u , [\(3.26\)](#) ($w_c^\top f_u \neq 0$), we construct the washout filter and feedback as

$$(3.29) \quad \dot{y}_{\text{wo}} = u, \quad u = K_{\text{st}}y + K_{\text{wo}}y_{\text{wo}}$$

(setting $y_{\text{ref}} = y_{\text{wo,ref}} = 0$ without loss of generality). If K_{st} and K_{wo} are of order $O(1)$, there exists a two-dimensional invariant slow manifold. The slow coordinates y and y_{wo} satisfy to first order the equation

$$\begin{aligned} \dot{y} &= \lambda_c[y - y_{\text{eq}}] + w_c^\top f_u [K_{\text{st}}y + K_{\text{wo}}y_{\text{wo}}] + O(\|(y - y_{\text{eq}}, u)\|^2), \\ \dot{y}_{\text{wo}} &= K_{\text{st}}y + K_{\text{wo}}y_{\text{wo}}, \end{aligned}$$

which has the Jacobian in the equilibrium $y = y_{\text{eq}}$, $u = 0$

$$A_{\text{wo}} = \begin{pmatrix} \lambda_c + w_c^\top f_u K_{\text{st}} & w_c^\top f_u K_{\text{wo}} \\ K_{\text{st}} & K_{\text{wo}} \end{pmatrix}.$$

Thus, the equilibrium is stable, if A_{wo} satisfies $\text{tr } A_{\text{wo}} = \lambda_c + K_{\text{wo}} + w_c^\top f_u K_{\text{st}} < 0$, $\det A_{\text{wo}} = \lambda_c K_{\text{wo}} > 0$, which are equivalent to

$$(3.30) \quad \lambda_c + K_{\text{wo}} < (-w_c^\top f_u)K_{\text{st}}, \quad K_{\text{wo}} > 0, \quad \text{if } x_{\text{eq}} \text{ is unstable } (\lambda_c > 0),$$

$$(3.31) \quad \lambda_c + K_{\text{wo}} < (-w_c^\top f_u)K_{\text{st}}, \quad K_{\text{wo}} < 0, \quad \text{if } x_{\text{eq}} \text{ is stable } (\lambda_c < 0).$$

Thus, the sign of K_{wo} has to be chosen depending on the stability of the branch (with arbitrary modulus, e.g., $K_{\text{wo}} = \pm 1$). After choosing the sign of K_{st} suitably, then the modulus of K_{st} has to be chosen sufficiently large. Consequently, a sufficient non-degeneracy condition for the existence of stabilizing gains ($K_{\text{st}}, K_{\text{wo}}$) is that

$$(3.32) \quad \lambda_c \neq 0.$$

It is also clear that A_{wo} is singular if $\lambda_c = 0$ such that the non-invasive feedback control based on washout filter fails for all possible gains at fold bifurcations (when $\lambda_c = 0$).

3.4.2. Non-invasive control through the bifurcation parameter. The general principle was discussed in [Subsection 3.3.2](#). We do not assume the presence of an input u in the right-hand side (thus, $\dot{x} = f(x, \mu, 0)$, $y = g(x)$), but require partial controllability through the bifurcation parameter μ , [\(3.27\)](#) ($w_c^\top f_\mu \neq 0$), and set

$$(3.33) \quad \dot{\mu} = u = K_{\text{st},y}[y - y_{\text{ref}}] + K_{\text{st},\mu}[\mu - \mu_{\text{ref}}].$$

If $K_{st,y}$ and $K_{st,\mu}$ are of order $O(1)$, and y_{ref} and μ_{ref} are near y_{eq} and μ_{eq} , there exists a two-dimensional invariant slow manifold. The slow coordinates y and μ satisfy to first order the equation

$$\begin{aligned}\dot{y} &= \lambda_c [y - y_{\text{eq}}] + w_c^\top f_\mu [\mu - \mu_{\text{eq}}] + O(\|(y - y_{\text{eq}}, \mu - \mu_{\text{eq}})\|^2), \\ \dot{\mu} &= K_{st,y} [y - y_{\text{ref}}] + K_{st,\mu} [\mu - \mu_{\text{ref}}],\end{aligned}$$

which has the Jacobian in the equilibrium $(x_{\text{eq}}, \mu_{\text{eq}})$

$$A_\mu = \begin{pmatrix} \lambda_c & w_c^\top f_\mu \\ K_{st,y} & K_{st,\mu} \end{pmatrix}.$$

Thus, criteria for stabilizing gains are that

$$(3.34) \quad K_{st,\mu} < -\lambda_c, \quad \lambda_c K_{st,\mu} - (w_c^\top f_\mu) K_{st,y} > 0.$$

Consequently, a sufficient non-degeneracy condition for the existence of stabilizing gains $(K_{st,y}, K_{st,\mu})$ is that

$$(3.35) \quad w_c^\top f_\mu \neq 0 \quad \text{or} \quad \lambda_c < 0,$$

If the equilibrium is part of a branch $(x_{\text{eq}}(s), \mu_{\text{eq}}(s))$, then the ratio $(\lambda_c)/(w_c^\top f_\mu)$ present in the second condition in (3.34) has a geometric interpretation under one additional assumption: differentiating the identity for equilibria, $f(x_{\text{eq}}(s), \mu_{\text{eq}}(s)) = 0$, with respect to s and projecting the resulting linear relation between $\partial_s x_{\text{eq}}$ and $\partial_s \mu_{\text{eq}}$ by w_c^\top , we obtain the linear relation

$$(3.36) \quad \lambda_c w_c^\top \partial_s x_{\text{eq}} + (w_c^\top f_\mu) \partial_s \mu_{\text{eq}} = 0.$$

If we assume in addition that the spectral stable projection of f_μ is not large, that is,

$$(3.37) \quad [I - v_c w_c^\top] f_\mu = O(1),$$

($[I - v_c w_c^\top]$ is the spectral projection for f_x onto $\ker w_c^\top$) then, by [Assumption 3.2](#), stability of $f_x|_{\ker w_c^\top}$ with timescale $1/\epsilon$, (3.23), $[I - v_c w_c^\top] \partial_s x_{\text{eq}} = [f_x|_{\ker w_c^\top}]^{-1} [I - v_c w_c^\top] f_\mu = O(\epsilon) \ll 1$. Consequently,

$$(3.38) \quad \partial_s y_{\text{eq}} = g_x \partial_s x_{\text{eq}} = g_x v_c w_c^\top \partial_s x_{\text{eq}} + O(\epsilon) = w_c^\top \partial_s x_{\text{eq}} + O(\epsilon).$$

Inserting $\partial_s y_{\text{eq}}$ for $w_c^\top \partial_s x_{\text{eq}}$ in (3.36), results in the relation

$$(3.39) \quad \lambda_c \partial_s y_{\text{eq}} + (w_c^\top f_\mu) \partial_s \mu_{\text{eq}} = O(\epsilon).$$

Thus, the second condition on the gains to be stabilizing can be phrased in terms of the tangent of the equilibrium curve in the (y, μ) -plane, $(y_{\text{eq}}(s), \mu_{\text{eq}}(s))$. The two vectors $(\lambda_c, w_c^\top f_\mu)$ and $(\partial_s y_{\text{eq}}, \partial_s \mu_{\text{eq}})$ are both non-zero and approximately orthogonal to each other along the equilibrium branch. Along a stable part of the equilibrium branch (where $\lambda_c < 0$ and the signs of $\partial_s y_{\text{eq}}$ and $\partial_s \mu_{\text{eq}}$ can be established with zero control gains), we may establish a sign $\sigma = \pm 1$

(independent of s) such that there exists a $p(s) > 0$ with $(\lambda_c, w_c^\top f_\mu) = p\sigma(\partial_s \mu_{\text{eq}}, -\partial_s y_{\text{eq}}) + O(\epsilon)$ for all $s \in [s_{\min}, s_{\max}]$. Thus, overall the criteria for the gains are

$$(3.40) \quad K_{\text{st},\mu} < -\lambda_c, \quad \sigma [\partial_s \mu_{\text{eq}} K_{\text{st},\mu} + \partial_s y_{\text{eq}} K_{\text{st},y}] + O(\epsilon) > 0.$$

In other words, the gains $(K_{\text{st},y}, K_{\text{st},\mu})$ need to be sufficiently large in modulus and the line in the (y, μ) plane defined by $0 = u = K_{\text{st},y}[y - y_{\text{ref}}] + K_{\text{st},\mu}[\mu - \mu_{\text{ref}}]$ must intersect the equilibrium curve $(y_{\text{eq}}(s), \mu_{\text{eq}}(s))$ at a non-zero angle. The orientation is determined by σ , such that we call the sign σ the *input orientation*.

The additional condition (3.37) is best understood by its primary consequence (3.38). The tangent to the equilibrium curve $(x_{\text{eq}}(s), \mu_{\text{eq}}(s))$ should be mostly tangential to the (y, μ) -plane. Thus, changes in equilibrium location and slow dynamics should be approximately aligned. This condition is known to be satisfied at a fold bifurcation in μ .

3.4.3. Non-invasive control based on zero-in-equilibrium feedback. The general principle was discussed in Subsection 3.3.3. The difference to Subsection 3.4.2 is that the input u in the right-hand side is present, such that $\dot{x} = f(x, \mu, au)$ with non-zero a , $y = g(x(t))$. We set, identically to Eq. (3.33),

$$(3.41) \quad \dot{\mu} = u, \quad u = K_{\text{st},y}[y - y_{\text{ref}}] + K_{\text{st},\mu}[\mu - \mu_{\text{ref}}].$$

If a , $K_{\text{st},y}$ and $K_{\text{st},\mu}$ are of order $O(1)$, and y_{ref} and μ_{ref} are near y_{eq} and μ_{eq} , there exists a two-dimensional invariant slow manifold. The slow coordinates y and μ satisfy to first order the equation

$$(3.42) \quad \begin{aligned} \dot{y} &= \lambda_c [y - y_{\text{eq}}] + w_c^\top f_\mu [\mu - \mu_{\text{ref}}] + aw_c^\top f_u [K_{\text{st},y}[y - y_{\text{ref}}] + K_{\text{st},\mu}[\mu - \mu_{\text{ref}}]] \\ &\quad + O(\|(y - y_{\text{eq}}, \mu - \mu_{\text{eq}})\|^2), \\ \dot{\mu} &= K_{\text{st},y}[y - y_{\text{ref}}] + K_{\text{st},\mu}[\mu - \mu_{\text{ref}}], \end{aligned}$$

which has the Jacobian in the equilibrium $(x_{\text{eq}}, \mu_{\text{eq}})$

$$A_{\text{ZIE}} = \begin{pmatrix} \lambda_c + aw_c^\top f_u K_{\text{st},y} & w_c^\top f_\mu + aw_c^\top f_u K_{\text{st},\mu} \\ K_{\text{st},y} & K_{\text{st},\mu} \end{pmatrix}.$$

Thus, criteria for stabilizing gains are that

$$(3.43) \quad K_{\text{st},\mu} + aw_c^\top f_u K_{\text{st},y} < -\lambda_c, \quad \lambda_c K_{\text{st},\mu} - w_c^\top f_\mu K_{\text{st},y} > 0.$$

Consequently, a sufficient non-degeneracy condition for the existence of stabilizing gains $(a, K_{\text{st},y}, K_{\text{st},\mu})$ is that

$$(3.44) \quad w_c^\top f_\mu \neq 0 \quad \text{or} \quad (\lambda_c \neq 0 \quad \text{and} \quad w_c^\top f_u \neq 0) \quad \text{or} \quad \lambda_c < 0,$$

which is violated only at events of codimension 2 (if $\lambda_c < 0$, $K_{\text{st},y} = K_{\text{st},\mu} = 0$ stabilizes such that the condition $w_c^\top f_\mu \neq 0$ is not necessary in that case). If one of the first two cases of (3.44) is satisfied, we can adjust the input scaling a such that the vectors $(1, aw_c^\top f_u)$ and

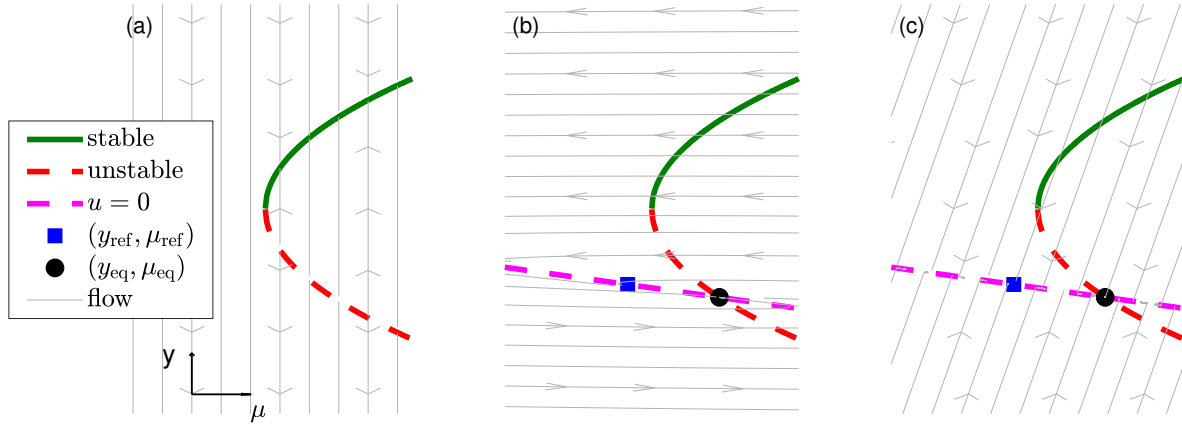


Figure 3.1. Illustration of the effect of different feedback control schemes on the flow. The stable (green) and unstable (red dashed) part of the equilibrium branch $(y_{\text{eq}}(s), \mu_{\text{eq}}(s))$ with the line $\{(y, \mu) : u = K_{\text{st},y}(y - y_{\text{ref}}) + K_{\text{st},\mu}(\mu - \mu_{\text{ref}}) = 0\}$ (dashed magenta) intersect in an equilibrium $(y_{\text{eq}}, \mu_{\text{eq}})$ (black circle) for suitable gains $(K_{\text{st},y}, K_{\text{st},\mu})$ and reference point $(y_{\text{ref}}, \mu_{\text{ref}})$ (blue square). Panel (a): uncontrolled system. Panel (b): control through bifurcation parameter in the case $|K_{\text{st},\mu}|, |K_{\text{st},y}| \gg 1$ used by [6] (grey arrows are fast). Panel (c): zero-in-equilibrium control in the case $|a| \gg 1$ (grey arrows are fast). The horizontal axis is μ and the vertical axis is y as is convention for bifurcation diagrams.

$(\lambda_c, -w_c^\top f_\mu)$ are linearly independent. Then the gains $(K_{\text{st},y}, K_{\text{st},\mu})$ can be chosen from the quadrant defined by the two affine inequalities in (3.43). The second condition on the gains in (3.43) is identical to the condition for control through only the bifurcation parameter, (3.33). Thus, it can be approximated by a geometric condition, such that we obtain the approximate criteria

$$(3.45) \quad K_{\text{st},\mu} + a w_c^\top f_u K_{\text{st},y} < -\lambda_c, \quad \sigma [\partial_s \mu_{\text{eq}} K_{\text{st},\mu} + \partial_s y_{\text{eq}} K_{\text{st},y}] + O(\epsilon) > 0.$$

Figure 3.1 illustrates how feedback control through the bifurcation parameter and zero-in-equilibrium affect the flow to stabilize unstable equilibria. Figure 3.1(a) shows an equilibrium branch $(y_{\text{eq}}(s), \mu_{\text{eq}}(s))$ with saddle-node bifurcation without control (System (3.42) with $K_{\text{st},y} = K_{\text{st},\mu} = 0$). The flow is indicated by grey arrows.

Figure 3.1(b) shows the effect of control through bifurcation parameter, which is a special case of zero-in-equilibrium feedback for $a = 0$. The sketch shows the case of large gains $(|K_{\text{st},y}|, |K_{\text{st},\mu}| \gg 1)$, which approximates the feedback rule (3.15), $\mu(t) = \mu_{\text{ref}} + K_{\text{st}}(y - y_{\text{ref}})$. The large gains cause the controlled flow to be slow-fast. In Figure 3.1(b,c) the grey arrows indicate the direction of the fast flow. The slow flow (not indicated in Figure 3.1(b,c)) then follows the line $\{u = 0\}$ (dashed, magenta) toward the equilibrium $(y_{\text{eq}}, \mu_{\text{eq}})$ (black circle). For the large-gain regime the fast flow is nearly horizontal (exclusively changing μ), causing large corrections in μ . For smaller gains $K_{\text{st},y}, K_{\text{st},\mu}$ trajectories of the controlled system may spiral, crossing the line $\{u = 0\}$ (dashed magenta), vertically, but eventually (for suitable gains) converging to the equilibrium $(y_{\text{eq}}, \mu_{\text{eq}})$ (black circle) which lies in the intersection of the line $u = 0$ and the equilibrium curve.

Figure 3.1(c) shows the effect of zero-in-equilibrium control ($a \neq 0$), emphasizing its effect by choosing $|a| \gg 1$. Again, the large parameter makes the controlled flow slow-fast. However, for zero-in-equilibrium control the fast flow is nearly parallel to the lines $\{\mu = \text{const}\}$. Thus, the control gain a enables control without large deviations in the parameter μ . This is beneficial for pedestrian flow control in a physical experiment, where the parameter is the location of the obstacle where large parameter variations correspond to large-amplitude motions of the obstacle with real-time requirements. Figure 5.4 in subsection 5.2 also shows that even for the pedestrian flow simulation the required size of gains for control through the bifurcation parameter pushes the simulation out of the regime where one may assume that there is only one slow dimension (see Assumption 3.2).

Criterion (3.43) expresses this advantage of zero-in-equilibrium control over control purely through the bifurcation parameter μ (corresponding to $a = 0$) quantitatively. If the coefficient $w_c^\top f_\mu$ is relatively small compared to $\lambda_c > 0$ (so the system does not react quickly to changes in μ along an unstable branch), the corrections by feedback control through μ (in $\dot{\mu} = u$) have to be large when $a = 0$, because $K_{st,\mu} < -\lambda_c$ is required when $a = 0$, which implies $\lambda_c K_{st,\mu} < -\lambda_c^2$, such that $|K_{st,y}| > \lambda_c^2 / |w_c^\top f_\mu|$ is required, which can be large, resulting in large right-hand sides for $\dot{\mu} = u$ in the presence of small disturbances. Geometrically this means that the line $\{u = 0\}$ in Figure 3.1(b) would be almost horizontal, resulting in trajectories of the controlled flow that are also almost horizontal (grey lines in Figure 3.1(b)) leading to large corrections in μ . On the other hand, the additional input au in the right-hand side of f with a (possibly large) scaling a of suitable sign permits us to satisfy the first criterion in (3.43) with a gain $K_{st,y}$ of arbitrary small modulus and $K_{st,\mu} > 0$, such that the second criterion is also satisfied (thus, most control is exerted through the input u in the right-hand side f). Figure 3.1(c) shows that even for a nearly horizontal line $\{u = 0\}$ (required if $|w_c^\top f_\mu| \ll 1$) the controlled flow does not show large excursions in the parameter μ , converging well to its equilibrium.

The particle-flow model for the pedestrian evacuation scenario introduced in Section 4 has this feature: controlling the flow by shifting the obstacle in x -direction requires large control action to compensate small disturbances. The additional input applies to each pedestrian a biasing force, with a strong direct effect on the output flux measures, such that the relative weighting between the control inputs is $a = 50$ (see Subsection 4.3.3).

4. Pedestrian Evacuation Scenario. In this section we describe a prototype multi-particle model for an evacuation scenario. We refer to it as a microscopic model, as we set the rules for the dynamics at the level of individual pedestrians. As mentioned in Subsection 2.2, the system exhibits tipping, a sudden change from one stable state to another stable state, and hysteresis, which we will analyze with non-invasive feedback control. We will treat the microscopic model like a physical experiment in the sense that we assume similar limitations. In particular, the microscopic state of the system is not set 'at will' and precise derivative information is not available.

4.1. General Set-up. It is assumed that pedestrians want to evacuate a building, passing through a corridor with an obstacle, as shown in Figure 4.1. To exit the building via the corridor, pedestrians have to choose which route they want to follow to maneuver around the obstacle. This choice is influenced by the shortest way to the exit and by the walking behavior

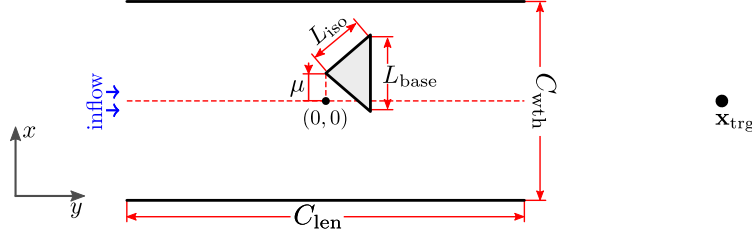


Figure 4.1. Geometry of corridor, obstacle and inflow area of pedestrians. See Table A.1 for values of the parameters for corridor and obstacle geometry.

of nearby pedestrians. The route choice behavior is investigated by changing the position of the obstacle and, thus, the preference for each route.

Social force model with lemming effect. We consider a scenario with N pedestrians, where N is large. Helbing and Molnar proposed a model in [19] where each pedestrian i is described by a particle of zero extent at position $\mathbf{x}_i(t)$ and moving with velocity $\dot{\mathbf{x}}_i(t)$ in the plane. Their motion is the response to forces acting on it. The so-called *social force model* assumes that the main forces that determine the motion of pedestrian i are their tendencies to do the following.

- Pedestrian i moves towards a target point $\mathbf{x}_{\text{trg}} \in \mathbb{R}^2$ (see Figure 4.1) aiming for a desired speed v_{trg} . This results in a target attraction force $\mathbf{F}_{\text{trg},i}$ acting on pedestrian i .
- Pedestrian i avoids close encounters with pedestrian j (for all $j \neq i, j \leq N$), resulting in a repulsive force $\mathbf{F}_{\text{rep},ij}^{\text{ped}}$.
- Pedestrian i avoids collision with each object j , which can be an obstacle or wall, resulting in a repulsive force $\mathbf{F}_{\text{rep},ij}^{\text{obj}}$.

The target attraction force is

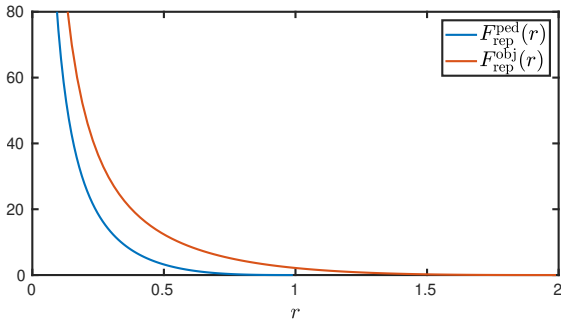
$$(4.1) \quad \mathbf{F}_{\text{trg},i} = \frac{1}{\tau} (v_{\text{trg}} \mathbf{e}_{\text{trg},i} - \dot{\mathbf{x}}(t)), \quad \text{where} \quad \mathbf{e}_{\text{trg},i} = \frac{\mathbf{x}_{\text{trg}} - \mathbf{x}_i}{\|\mathbf{x}_{\text{trg}} - \mathbf{x}_i\|}$$

is the direction vector toward the target point \mathbf{x}_{trg} and τ is the reaction time. In our case all pedestrians have the same target point and reaction time (see Table A.1). The force $\mathbf{F}_{\text{trg},i}$ such that, in the absence of other pedestrians or obstacles, pedestrian i adjusts their velocity with rate τ such that they move with speed v_{trg} toward \mathbf{x}_{trg} . The repulsive forces from other pedestrians and from objects are modeled as monotonic decreasing functions of the distance to other pedestrians and obstacles respectively. Following [28], we make the following choice for pedestrian-pedestrian (superscript $s = \text{ped}$) and pedestrian-obstacle/wall (superscript $s = \text{obj}$) interactions forces:

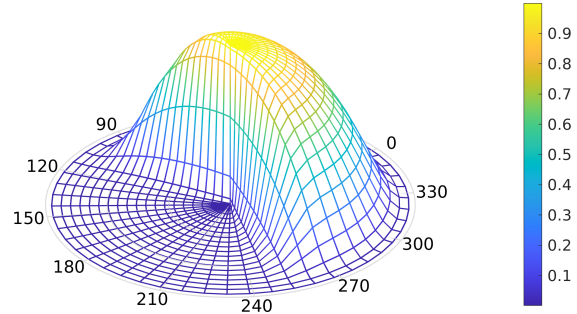
$$(4.2) \quad \mathbf{F}_{\text{rep},ij}^s = F_{\text{rep}}^s(\|\mathbf{r}_{ij}\|) \frac{\mathbf{r}_{ij}}{\|\mathbf{r}_{ij}\|}, \quad \text{with} \quad F_{\text{rep}}^s(r) = \begin{cases} -V_{\text{rep}}^s [\tan g^s(r) - g^s(r)] & \text{if } r < \sigma^s, \\ 0 & \text{if } r \geq \sigma^s, \end{cases} \quad \text{and} \\ g^s(r) = \frac{\pi}{2} \left(\frac{r}{\sigma^s} - 1 \right) \quad \text{for } s = \text{obj or ped}.$$

Here $\mathbf{r}_{ij} = \mathbf{x}_j - \mathbf{x}_i$ is the vector between pedestrian i and pedestrian (or obstacle) j . For the case of an obstacle (wall or triangle), this vector is defined as pointing toward the point of the obstacle j that is closest to the pedestrian i . The parameters $V_{\text{rep}}^{\text{ped}}$ and $V_{\text{rep}}^{\text{obj}}$ control the repulsion strength between pedestrians, or between pedestrians and obstacles, respectively (chosen uniform for all pedestrians and obstacles here). The repulsion force is radially symmetric and has finite range, in contrast to [19]. Figure 4.2a shows its dependence on the distance $r = \|\mathbf{r}_{ij}\|$ between particles or objects i and j . So, the equation of motion for pedestrian $i \leq N$ according to the social force model is given by

$$\ddot{\mathbf{x}}_i = \mathbf{F}_{\text{trg},i} + \sum_{j=1}^N \mathbf{F}_{\text{rep},ij}^{\text{ped}} + \sum_{\text{objects } k} \mathbf{F}_{\text{rep},ik}^{\text{obj}} \quad (\text{social force model}).$$



(a) Graphs of repulsive force $F_{\text{rep}}^s(r)$ in (4.2), for $s \in \{\text{ped}, \text{obj}\}$. The function $F_{\text{rep}}^s(r)$ is zero for $r \geq \sigma^s$.



(b) Alignment weighting $\kappa(r, \theta)$ in (4.4), shown as a graph of the complex argument $r \exp(i\theta)$.

Figure 4.2. Graphs of interaction forces for repulsion (Figure 4.2a) and alignment (Figure 4.2b). In Figure 4.2b the radial component is the distance of pedestrian j from i , the angular component is the difference of their angular velocity. See Table A.1 for parameter values.

Starke *et al.* [40] hypothesize the presence of another force, namely a tendency to follow others. For example, this effect may be present in an emergency situation when there is no good knowledge of the geometry of the building. In such a situation pedestrian i has a preference to move in the same direction as other pedestrian around him. This psychological factor was called the *lemming effect* in [40] and was modeled by changing the directional vector in $\mathbf{F}_{\text{trg},i}$ to a linear combination of the direction $\mathbf{e}_{\text{trg},i}$ towards the target point \mathbf{x}_{trg} and a weighted mean velocity $\langle \mathbf{v} \rangle_i$ of the velocity vectors $\mathbf{v}_j = \dot{\mathbf{x}}_j$ of pedestrians j in a neighborhood of pedestrian i :

$$(4.3) \quad \mathbf{e}_{\text{al},i}(t) = \frac{(1 - p_{\text{al}})\mathbf{e}_{\text{trg},i} + p_{\text{al}}\langle \mathbf{v} \rangle_i}{\|(1 - p_{\text{al}})\mathbf{e}_{\text{trg},i} + p_{\text{al}}\langle \mathbf{v} \rangle_i\|}, \quad \text{where} \quad \langle \mathbf{v} \rangle_i = \frac{\sum_{j \neq i} \kappa(\|\mathbf{r}_{ij}\|, \angle \dot{\mathbf{r}}_{ij}) \mathbf{v}_j(t)}{\sum_{j \neq i} \kappa(\|\mathbf{r}_{ij}\|, \angle \dot{\mathbf{r}}_{ij})},$$

and $p_{\text{al}} \in [0, 1]$ denotes the *lemming parameter* which controls the influence other pedestrians have over the target direction. The weight function $\kappa(r, \theta)$ depends on the distance $r = \|\mathbf{r}_{ij}\|$ of pedestrians i and j and the angle $\theta = \angle \dot{\mathbf{r}}_{ij} = \angle \dot{\mathbf{x}}_j - \angle \dot{\mathbf{x}}_i$ between their walking directions

(their velocity vectors). The quantity $\langle \mathbf{v} \rangle_i$ is called the weighted mean velocity vector. It depends on weights determined by the real-valued weighting function

$$(4.4) \quad \kappa(r, \theta) = \begin{cases} \frac{\gamma}{1 + \exp(-\alpha \cos(\beta\theta))} \exp\left(\frac{\sigma_{\text{al}}^2}{r^2 - \sigma_{\text{al}}^2}\right) & \text{if } r \leq \sigma_{\text{al}}, \\ 0 & \text{if } r > \sigma_{\text{al}} \end{cases} \quad \text{for } r \geq 0, \theta \in [-\pi, \pi].$$

The weight function κ has a finite support radius σ_{al} for r . The parameter γ is a scaling factor, and parameters α and β are chosen such that each pedestrian is influenced by pedestrians nearby, walking in the same direction. More precisely, each pedestrian is influenced by others walking in approximately the same directions (κ is noticeably positive for angles $\theta \in [-100^\circ, 100^\circ]$ and for $r < \sigma_{\text{al}}$, see [Figure 4.2b](#)). Assuming that pedestrian i is placed in the center, the graph in [Figure 4.2b](#) indicates how much another pedestrian j inside the finite support radius influences the mean $\langle \mathbf{v} \rangle_i$ depending on their relative walking direction.

Consequently, the target attraction force is modified to take into account the tendency for alignment, such that we modify our social force model. The equation of motion for pedestrian i is given by

$$(4.5) \quad \ddot{\mathbf{x}}_i = \mathbf{F}_{\text{al},i} + \sum_{j=1}^N \mathbf{F}_{\text{rep},ij}^{\text{ped}} + \sum_{\text{objects } k} \mathbf{F}_{\text{rep},ik}^{\text{obj}} \quad (\text{social force model with alignment}), \text{ where}$$

$$\mathbf{F}_{\text{al},i} = \frac{1}{\tau} (v_{\text{trg}} \mathbf{e}_{\text{al},i} - \dot{\mathbf{x}}(t)),$$

and $\mathbf{e}_{\text{al},i}$ is defined in [\(4.3\)](#), and $\mathbf{F}_{\text{rep},ij}^{\text{ped}}$ and $\mathbf{F}_{\text{rep},ik}^{\text{obj}}$ are defined in [\(4.2\)](#).

4.2. Bistable behavior and hysteresis. In the following, we consider model [\(4.5\)](#) with $N = 100$ pedestrians in the corridor. The boundary conditions are such that for every pedestrian exiting the corridor at $y = C_{\text{len}}/2$, a new pedestrian enters at $y = -C_{\text{len}}/2$ with initial velocity $(v_{\text{trg}}, 0)$ and with a vertical position uniformly randomly distributed around the center line of the corridor within the interval $[-0.5, 0.5]$. The values of the remaining parameters can be found in [Table A.1](#). The number of pedestrians is chosen so that the crowd in the corridor is of medium density, too many pedestrians would overcrowd the corridor while too little would result in an interrupted flow. The system parameter which we vary to perform the bifurcation analysis is the position of the tip of the triangular obstacle μ as shown in [Figure 4.1](#).

Details of simulation protocol for [Figure 2.1\(b\)](#). Starting with $\mu = -1.2$ m, the system was numerically integrated (see [Appendix A](#) for details of integration). The parameter μ was increased in steps of 0.1 meters every 300 seconds, so we were slowly changing the position of the tip of the triangle performing a quasi-stationary *up-sweep*. When $\mu = 1.2$ m, we started decreasing it in steps of 0.1 m until the triangle was at its original position ($\mu = -1.2$ m) performing a *down-sweep*.

Reproducing the results of [\[40\]](#), we confirmed that the system exhibits bistability and hysteresis, as shown in [Figure 2.1\(b\)](#). The macroscopic variable used for the y -axis in [Figure 2.1\(b\)](#) is the difference of fluxes $\Delta\Phi = \Phi_+ - \Phi_-$ at each side of the obstacle. In [Figure 2.1\(b\)](#), the fluxes Φ_+ and Φ_- are measured as the number of pedestrians passing the end of the obstacle.

More precisely,

$$(4.6) \quad \Delta\Phi(t) = \frac{1}{\tau_{\max}} \int_{t-\tau_{\max}}^t (\Phi_+(s) - \Phi_-(s)) ds, \quad \text{where}$$

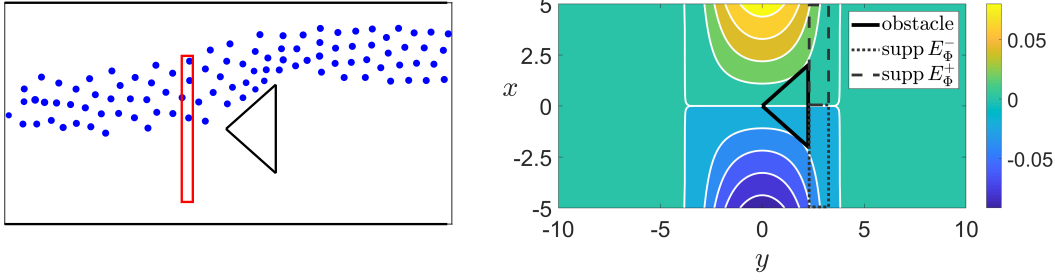
$$\Phi_{\pm}(t) = \sum_{i=1}^N E_{\Phi}^{\pm}(\mathbf{x}_i(t)), \quad \text{and} \quad E_{\Phi}^{\pm}(x, y) = \begin{cases} 1 & \text{if } \pm(x - \mu) > 0 \text{ and } |y - y_{c,\Phi}| \leq y_{\text{len},\Phi}, \\ 0 & \text{otherwise.} \end{cases}$$

Thus, $\Phi_{\pm}(t)$ is the number of pedestrians with position $\mathbf{x}_i(t) = (x_i(t), y_i(t))$ in a spatial box given by $|y_i - y_{c,\Phi}| \leq y_{\text{len},\Phi}$ and $x_i > \mu$ for Φ_+ or $x_i < \mu$ for Φ_- (see also [Figure 4.3b](#)). The concrete parameters for our spatial box for counting are $y_{c,\Phi} = \sqrt{L_{\text{iso}}^2 - L_{\text{base}}^2}/4 + 0.5 \text{ m} = 2.5 \text{ m}$, $y_{\text{len},\Phi} = 0.5 \text{ m}$. The averaging interval length τ_{\max} for $\Delta\Phi(t)$ is 10 seconds. In [Figure 2.1\(b\)](#), the value of $\Delta\Phi = \Phi_+ - \Phi_-$ at the end of the 300 s interval, just before we change the position of the obstacle μ , is plotted for each value of μ . The two overlapping stable branches of steady flow states in [Figure 2.1\(b\)](#) are the result of this up-sweep and down-sweep of the parameter μ . At one value of μ for each sweep, the steady flow state jumps from one branch to the other. This hysteresis suggests the existence of an unstable branch of steady states that connects the stable ones at two saddle-node bifurcations.

4.3. Output and input for measurement and control. Due to the randomness of the x -coordinate at entry to the corridor, we can expect deterministic results in our system only in the limit number of pedestrians $N \rightarrow \infty$ with suitably scaled corridor and obstacle parameters $\mu, L_{\text{base}}, L_{\text{iso}}, C_{\text{len}}, C_{\text{wth}} \sim \sqrt{N}$. The fluctuations due to finite N make the averaging over time for the fluxes Φ_{\pm} necessary. The flux measure Φ_{\pm} has further disadvantages, especially if one plans to make a feedback control input depend on it to perform bifurcation analysis. The measure can only take a finite and small number of integer values. In addition, the results depend on the time window size for the average, where one has a tradeoff. A small time window results in large fluctuations, while a large window averages out important system characteristics and may introduce a delay into the control feedback loop.

4.3.1. Instantaneous space-averaged flux measure. We introduce a space-averaged flux measure ϕ , which is instantaneous. This means that the measure $\phi(t)$ depends only on the vector $(\mathbf{x}(t), \dot{\mathbf{x}}(t))$, not a history $\tau \mapsto (\mathbf{x}(t + \tau), \dot{\mathbf{x}}(t + \tau))$ for τ in some interval $[-\tau_{\max}, 0]$ (in contrast to $\Phi_{\pm}(t)$, where $\tau_{\max} = 10 \text{ s}$).

The space average has a weight kernel $w_{\text{pos}}(x, y)$ such that every pedestrian counts with a weight according to their position. The contribution of each pedestrian to the flux is the product of this value with its velocity component $v_i^x(t)$ along the corridor. Denote the state space vector for pedestrian i by $\mathbf{X}_i(t) = (\mathbf{x}_i(t), \dot{\mathbf{x}}_i(t)) = (x_i(t), y_i(t), v_i^x(t), v_i^y(t))$, and the overall state space vector by $\mathbf{X}(t) = (\mathbf{X}_1(t), \dots, \mathbf{X}_N(t))$ at time t . Then the flux ϕ is defined



(a) Control signal u acts as bias force on pedestrians in red box in front of obstacle, where $b(x, y) \neq 0$ in (4.10).

(b) Color: weight w_{pos} for pedestrian positions in space averaged flux measure ϕ ; Dashed and dotted boxes: area where $E_{\Phi}^{\pm} \neq 0$ in (4.6).

Figure 4.3. Area for input (Figure 4.3a), and weight function $w_{\text{pos}}(x, y)$ for instantaneous flux measure, given in (4.8). At $y = 0$, $w_{\text{pos}}(\cdot, 0)$ decreases linearly in x (maximal at upper wall, here $x = 5$, minimal at lower, $x = -5$). Figure 4.3b also shows the boxes $E_{\Phi}^{\pm}(x, y)$ used for counting in flux measure Φ_{\pm} in (4.6).

as

$$(4.7) \quad \phi(\mathbf{X}(t)) = \sum_{i=1}^N w_{\text{pos}}(x_i(t), y_i(t)) v_i^x(t), \text{ with}$$

$$(4.8) \quad w_{\text{pos}}(x, y) = E(x, r_+(x, y)) - E(x, r_-(x, y)), \quad E(x, r) = \begin{cases} \eta|x| \int_0^{\infty} \frac{e^{-t}}{t} dt & \text{if } |r| < d \\ \frac{d^2}{d^2 - r^2} & \text{if } |r| \geq d, \end{cases}$$

$$r_{\pm}^2(x, y) = (x \pm x_{c,\phi})^2 + (y - y_{c,\phi})^2.$$

The parameter $d = 4$ m is the length scale of the weight function w_{pos} and $\eta = (1/12) \text{ s/m}^3$ is a scaling factor which also makes the flux dimensionless. The weight function was chosen to have two bell shaped humps (one positive, one negative, see Figure 4.3b) with extrema at the points $(\pm x_{c,\phi}, y_{c,\phi}) = (\pm C_{\text{wth}}/2, 0)$ where pedestrian motion should be weighted highest: The y coordinate of the extrema, $y_{c,\phi}$ is the horizontal (y) position of the tip of the triangular obstacle ($y_{c,\phi} = 0$), while the weight increases linearly in x along the line $y = 0$.

Figure 4.4a repeats the result shown in Figure 2.1(b), but using the instantaneous flux measure ϕ in its y -axis. The underlying data is the same in Figure 2.1(b) such that the same bistability is observed. In Figure 4.4b, the time profile of the flux ϕ for $\mu = -1.2$ m is shown to illustrate the size and time scale of fluctuations and level of stationarity for a stable steady flow. Although at this position there is a stable and observable steady state, the flux exhibits large fluctuations because of the finite number N of pedestrians. For the value $\mu = -1.2$, for which Figure 4.4b is shown, a steady flow of pedestrians moving only on the right side of the obstacle is observed. The standard deviation through the last 20 seconds is 0.05, while the one for the whole time interval is 0.0418. This measure is used to estimate stationarity.

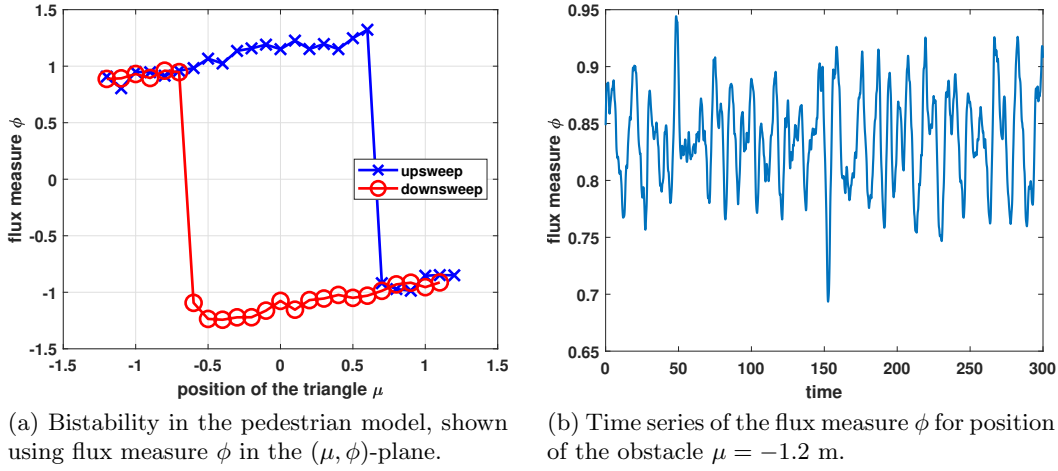


Figure 4.4. *Figure 4.4a shows same data and parameter sweep as Figure 2.1(b) but with different macroscopic measure: output is the value of space-averaged flux $\phi(t)$ at the end of each 300 s interval with fixed μ . At this point, we assume that the system has settled at a steady state with fluctuations, as shown in Figure 4.4b.*

4.3.2. Control input through bias force. For performing continuation on the evacuation scenario with feedback control as proposed in Subsections 3.4.1 and 3.4.3, we need to specify how the scalar control input u enters model (4.5). We also aim to choose an input that is feasible in the sense that could be applied similarly in a real-life experiment. The motivation comes from traffic control, where signage and traffic light is used to control or direct flows. For our specific scenario, a display showing arrows in front of the obstacle acts as the control input. Pedestrians close to the display see these arrows pointing left or right, where the size of the arrow depends on the control input u , while the arrows do not directly influence pedestrians that cannot see the display.

Let us recall the *social force model* (4.5). We add a linear scalar control input on the particles that induces a behavior similar to a reaction to displaying arrows to pedestrians:

$$(4.9) \quad \ddot{\mathbf{x}}_i = \mathbf{F}_{al,i} + \sum_{j=1}^N \mathbf{F}_{rep,ij}^{\text{ped}} + \sum_{\text{objects } k} \mathbf{F}_{rep,ik}^{\text{obj}} + \begin{bmatrix} b(\mathbf{x}_i) \\ 0 \end{bmatrix} au, \text{ where}$$

$$(4.10) \quad b(\mathbf{x}) = b(x, y) = \begin{cases} 1 & \text{if } |x - x_{c,b}| \leq x_{\text{wth},b}, |y - y_{c,b}| \leq y_{\text{len},b} \\ 0 & \text{otherwise,} \end{cases}$$

where u is the scalar time-dependent control input, and a is the scaling of the gains, as introduced for our zero-in-equilibrium feedback control (3.19) in Subsection 3.3.3. The parameters $(x_{c,b}, y_{c,b}) = (\mu, -1.75 \text{ m})$ and $(x_{\text{wth},b}, y_{\text{len},b}) = (3.3 \text{ m}, 0.25 \text{ m})$ define a box in which the factor b in front of the control u has non-zero support. This box is in front of the obstacle, as illustrated in Figure 4.3a (with red frame). It is the area where the pedestrian have visual contact with the monitor. The influence of the feedback control input u is zero outside of this box. The factor $(0, b)$ for au in (4.9) describes that, when a pedestrian is inside the control input support box, a bias force acts on them pushing perpendicular to the direction of the

corridor (in x -direction, see also [Figure 4.1](#)). When closing the feedback loop we permit the input u to depend on the output ϕ , the flux measure defined by [\(4.7\)](#).

4.3.3. Choice of control gains. Here we discuss the choice of gains $(a, K_{st,\mu}, K_{st,\phi})$ for the continuation of the particle flow model. Note that the subscript of the last gain (formerly $K_{st,y}$) is now ϕ to indicate that the output is ϕ as defined in [\(4.7\)](#). First, we make some assumptions based on experimental evidence, e.g. on the response of the system. Then, the choice of proper gains is possible by combining these assumptions with properties of the zero-in-equilibrium feedback control, see also [subsection 3.4.3](#).

Input orientation σ . The blue crosses and the red circles in [Figure 2.1\(c\)](#) show the stable parts of the equilibrium branch for the flux measure ϕ as observed during the parameter sweep, see [\(4.7\)](#) for the definition of ϕ . Hypothesizing a saddle-node bifurcations near the transitions and a single unstable connecting branch between the stable branches, the topology of the figures implies that the sign of the input orientation σ in [\(3.45\)](#) must be negative at the equilibrium curve at $\mu \approx -1.25$. Thus, $\sigma = -1$. Recall that σ determines the orientation between equilibrium curve tangent in the (μ, ϕ) -plane and the line $\dot{\mu} = 0$.

Input effect. Next, we determine the sign of the coefficient $w_c^\top f_u$ appearing in the conditions [\(3.45\)](#): By construction, the input u acts as a bias force, see [\(4.9\)](#), such that positive u has a direct effect on the flux measure ϕ with positive sign which indicates $w_c^\top f_u > 0$.

Control gains. With the signs of σ and $w_c^\top f_u$ as determined above, in order to satisfy the conditions in [\(3.45\)](#) we chose fixed values for the gains a and $K_{st,\phi}$. The parameter $K_{st,\mu}$ is adjusted in each continuation step such that, (a), it is bounded from above, and (b), the line defined in [\(3.41\)](#) is not parallel to the equilibrium curve. Recall that the secant vector $v = (v_\mu, v_\phi)$ is the approximation of the tangent to the equilibrium curve. In practice, we chose

$$(4.11) \quad a = 50, \quad K_{st,\phi} = -0.2, \quad |K_{st,\mu}| = 0.2 \frac{v_\mu}{v_\phi}.$$

Note that for $K_{st,\mu} = -0.2v_\mu/v_\phi$ the line $\dot{\mu} = 0$ is perpendicular to the secant vector v . However, close to the sign changes of v_ϕ (extrema in ϕ of the equilibrium curve), [\(4.11\)](#) may lead to a gain $K_{st,\mu}$ with large modulus and possibly positive sign, which can lead to violation of the first condition in [\(3.45\)](#).

In these cases, we chose $K_{st,\mu} = 0.2v_\mu/v_\phi$ and we confirmed that this choice of gains indeed stabilized the system so that we successfully tracked the equilibrium curve. In practice, we switched the sign of $K_{st,\mu}$ whenever during continuation the system was driven away from a reference point (μ_{ref}, ϕ_{ref}) by more than distance $r_\sigma = 0.2$. For $K_{st,\mu} = 0.2v_\mu/v_\phi$ the line $\dot{\mu} = 0$ is not perpendicular to the equilibrium curve. However, the second condition on the gains in [\(3.45\)](#) is still satisfied.

5. Control-based continuation of the pedestrian flux. In this section, we will test two of the proposed inherently non-invasive feedback control laws, namely the washout filter [\(3.7\)](#) and the zero-in-equilibrium feedback control introduced in [\(3.19\)](#). As already briefly discussed in [Subsection 3.4.3](#), while feedback control through the parameter (described in [Subsections 3.3.2](#) and [3.4.2](#)) should be also feasible and stabilizing, we observed that the control would have required large gains $(K_{st,\mu}, K_{st,y})$ that violated [Assumption 3.2](#) about the presence of only a single slow direction.

Hence, our setup has a control input u , given in (4.9), (4.10) in Subsection 4.3.2, separate from the also varying bifurcation parameter μ . This is similar to the driven-pendulum experiments performed by Bureau et al. [8], where control was also input through an external force, a real-time controllable magnet.

According to (3.29) in Subsection 3.4.1 for the washout filter we may set the factor $a = 1$ in (4.9) without loss of generality, and set

$$(5.1) \quad u(t) = K_{\text{st}}\phi(t) + K_{\text{wo}}y_{\text{wo}}(t), \quad \dot{y}_{\text{wo}} = u(t).$$

For zero-in-equilibrium feedback control, we keep a in (4.9) as an adjustable gain (fixed as given in (4.11)) and set, according to (3.41),

$$(5.2) \quad u(t) = K_{\text{st},\phi}[\phi(t) - \phi_{\text{ref}}] + K_{\text{st},\mu}[\mu - \mu_{\text{ref}}], \quad \dot{\mu} = u(t).$$

During continuation the reference values $(\phi_{\text{ref}}, \mu_{\text{ref}})$ in (5.2) are defined via a secant prediction.

Protocol for simulation with feedback control and determination of steady states. Along the continuation of a branch the simulation runs as a continuous computational experiment, numerically integrating (4.9) with (5.1) or (5.2). At certain times t_{set} some parameters and possibly the gains are set to values determined by the continuation. For the washout-filtered control law (5.1) these are the washout filter state $y_{\text{wo}}(t_{\text{set}})$ and obstacle μ , while the gains are kept fixed: $(K_{\text{st}}, K_{\text{wo}}) = (-5, \pm 0.1)$ with the sign of K_{wo} depending on the stability of the branch. For the general zero-in-equilibrium control law (5.2), the varying parameters and gains are $(\phi_{\text{ref}}, \mu_{\text{ref}})$ and $K_{\text{st},\mu}$ while $K_{\text{st},\phi}$ and a are fixed according to (4.11). After setting these parameters, the simulation is continued until it becomes stationary. At this point a steady state has been reached such that we record it, and determine new parameters $(\phi_{\text{ref}}, \mu_{\text{ref}})$ and $K_{\text{st},\mu}$.

Our condition determining that a steady state is reached is as follows. When integrating numerically the system (4.9), (5.1) or (5.2), we obtain a sequence $\phi_0, \phi_1, \phi_2, \dots, \phi_n$ of outputs after n integration steps. We assume that the output measure ϕ is stationary at time n when the standard deviation std_n of last n_{min} outputs, $(\phi_{n-n_{\text{min}}+1}, \dots, \phi_n)$, does not exceed a given tolerance tol_{std} . We choose $n_{\text{min}} = 200$ which corresponds to 20 seconds (time step is 0.1 s) and tolerance $\text{tol}_{\text{std}} = 0.05$. This choice takes into account that we expect from the law of large numbers that the fluctuations will have standard deviation $\sim 1/\sqrt{N}$ and is consistent with the observed standard deviation of the time series of the flux for the stable steady states, as shown in Figure 4.4b.

5.1. Results for control with washout filter. As expected by Lemma 3.1 the control using washout filters, (5.1), will be able to track a branch of unstable steady states if one exists. As Figure 5.1 demonstrates the control indeed settles to a steady state with fluctuations below tolerance for a range of fixed μ in the region of unstable states (see the red stars in Figure 5.1). In this region, as required by our analysis in Subsection 3.4.1, the gain K_{wo} had to be positive. We also recovered the two branches of steady states of the system when using control (5.1) and $K_{\text{wo}} < 0$, thus, the completing bifurcation diagram except for small regions near the transitions.

During the continuation of each branch at each step j (at time $t_{\text{set},j}$) we used a secant prediction $(\mu_{\text{pred},j}, \phi_{\text{pred},j})$ with a step size of $\Delta_{\text{cont}} = 0.1$. The parameter μ is then kept

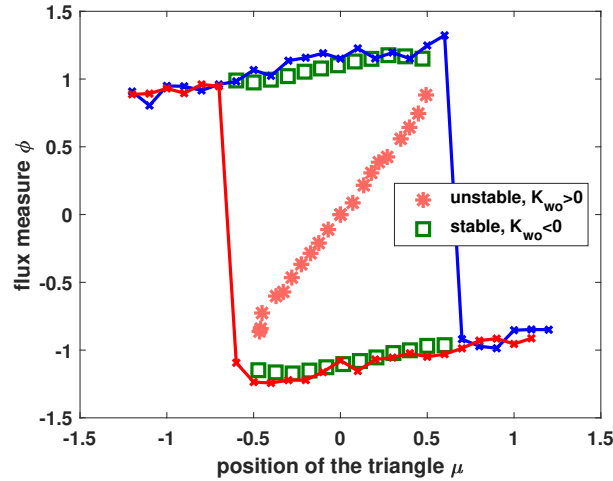


Figure 5.1. Bifurcation diagram of the evacuation scenario obtained by control through washout filters as given in (5.1). The red stars correspond to unstable steady states (tracked for $K_{wo} > 0$) and the green ones correspond to stable steady states ($K_{wo} < 0$). The blue and red lines show the observed steady states from sweeping the parameter μ (identical to Figure 4.4a). Control gains: $K_{st} = -5$, $K_{wo} = \pm 0.1$

constant at $\mu_{\text{pred},j}$ throughout the simulation and the initial value for the variable y_{wo} equals $y_{wo}(t_{\text{set},j}) = -\phi_{\text{pred},j}K_{st}/K_{wo}$, such that $u(t_{\text{set},j}) = 0$ at the starting time $t_{\text{set},j}$ of the simulation with new parameters. When the stationarity condition is satisfied we obtain the output, flux measure ϕ_j , determining the new approximate fixed point (μ_j, ϕ_j) with $\mu_j = \mu_{\text{pred},j}$. The result displayed at Figure 5.1 is computed in 3 pieces, as the control (5.1) fails to stabilize near the transition points.

The results shown in Figure 5.1 support the hypothesis that there is a unique unstable branch separating the stable branches in the region of bistability. The diagram suggests that the transition is a saddle-node (or fold) bifurcation but with the control (5.1), using the standard washout filters we are unable to track the branches near these transition points. As Lemma 3.1 shows, this type of control is singular close to folds in contrast to (5.2).

5.2. Results for zero-in-equilibrium feedback control. As expected by Lemma 3.3, zero-in-equilibrium feedback control, (5.2), succeeded in tracking the full bifurcation diagram of the underlying system. The results are demonstrated in Figure 5.2. At step j of the continuation (at time $t_{\text{set},j}$) the secant prediction for the next steady state is $(\mu_{\text{pred},j}, \phi_{\text{pred},j})$, which enters control law (5.2) as $(\mu_{\text{ref}}, \phi_{\text{ref}})$. The step size here is also $\Delta_{\text{cont}} = 0.1$. The slope of the line $\dot{\mu} = 0$ is determined by the gains $K_{st,\phi}$ and $K_{st,\mu}$, and chosen, as described in Subsection 3.4.3 and specified in (4.11), intersecting the equilibrium curve, and with $K_{st,\phi} = -0.2$. The large but fixed choice of gain scaling $a = 50$ in (4.11), with which u enters in (4.9), implies that feedback through the parameter is small in amplitude compared to the feedback through the input shown in Figure 4.3a.

Figure 5.2 also shows the lines $\dot{\mu} = 0$ (dashed magenta lines) for some steps of the continuation to illustrate the adjustment of control gain $K_{st,\mu}$. The cyan circles are the predictions $(\mu_{\text{pred},j}, \phi_{\text{pred},j})$ for each step j . The green squares and red stars are the accepted values for

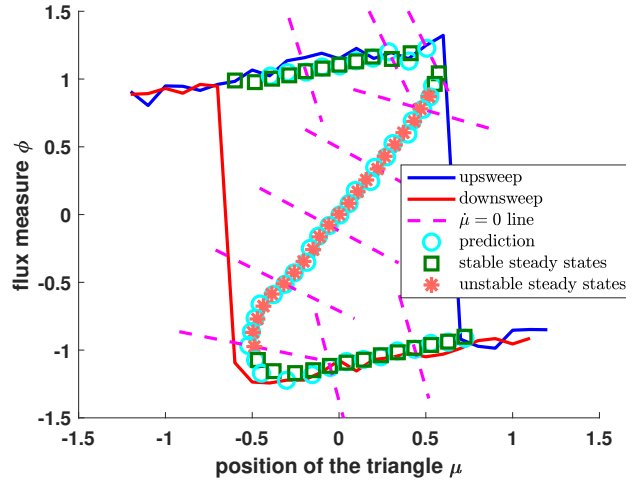


Figure 5.2. Bifurcation diagram of the evacuation scenario obtained by zero-in-equilibrium feedback control, (5.2). A family of equilibria is tracked through two saddle-node bifurcations. A predicted point $(\mu_{\text{ref}}, \phi_{\text{ref}})$ is marked with a cyan circle. The fixed gains are $(K_{\text{st},\phi}, a) = (-0.2, 50)$. The gain $K_{\text{st},\mu}$ is adjusted for each steady state. Its value is implied by the lines $\dot{\mu} = 0$ (only shown for a few selected points in magenta, dashed), see also (5.2) At each step of the continuation the steady state has to be on its $(\dot{\mu} = 0)$ -line. The blue and the red lines show the results of the parameter sweep.

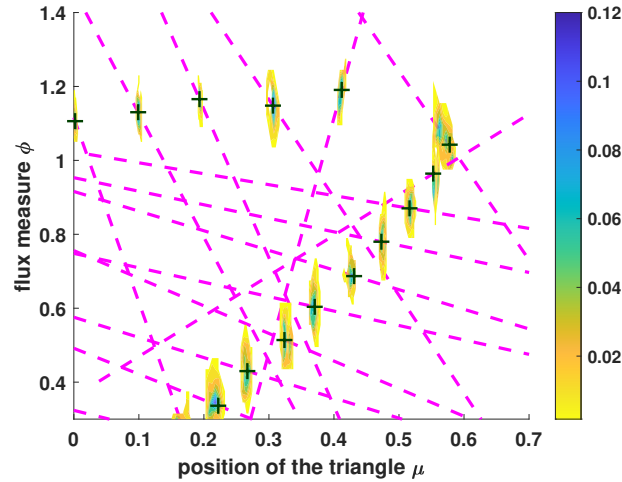


Figure 5.3. Results of zero-in-equilibrium feedback control close to the fold: evolution of the system in the (μ, ϕ) -plane throughout the procedure of tracking steady states close to the upper fold. The last 60 seconds of the trajectory $(\mu(t), \phi(t))$ are displayed. The accepted fixed points are shown as black crosses. The magenta dashed lines are the $\dot{\mu} = 0$ lines according to (5.2). The color code indicates the percentage of time spend at a position (μ, ϕ) .

an equilibrium as fluctuations dropped below tolerance. The green and red colors correspond to stable and unstable equilibria, respectively, as determined by the topology of the branch. For comparison, the blue and the red lines show the results of the parameter sweep (identical to Figure 4.4b).

Figure 5.3 shows additional details of the behavior of the system with control law (5.2) close to the upper fold point of the branch. The parameter μ changes dynamically throughout the simulation. For each fixed point, the dynamical system moves in the (μ, ϕ) -plane, eventually approaching a new steady state (ϕ_j, μ_j) . The feedback introducing dynamics for μ permits us to track solution branches around the fold bifurcation, as had been observed by [38]. Figure 5.3 shows the percentage of time spent at every position at the (μ, ϕ) -plane during the final 60 seconds before acceptance of the steady state on a color scale. Away from the fold the parameter μ is almost constant during transients, apart from the initial adjustment to $\mu_{\text{pred},j}$ (visible in the form of upright horizontally narrow color ellipses in Figure 5.3). However, when approaching the fold point, the variation in the μ direction becomes larger moving the parameter μ , thus highlighting that control through the parameter plays a role here, even though it is smaller by the factor $a = 50$ compared to the input u in (4.9). The lines $\dot{\mu} = 0$, required to be intersecting the branch for every step (dashed line in magenta), show where the new steady state should lie along the branch. We observe that during transients the evolution of the system in the (μ, ϕ) -plane does not stay on this line. The stabilization by the feedback control only implies that the system should converge to it.

Failure of control through the bifurcation parameter. After presenting the results of successfully implementing the classical washout filter and the zero-in-equilibrium feedback control that was introduced in this paper, we now briefly discuss results of experimentations with applying feedback control only through the parameter (described in Subsections 3.3.2 and 3.4.2) to stabilize the system.

Figure 5.4 shows projections of the controlled flow in the (μ, ϕ) plane when control is applied only through the bifurcation parameter μ near the known unstable equilibrium point $(\mu_{\text{eq}}(s_0), \phi_{\text{eq}}(s_0)) = (0, 0)$ and for various control gains $(K_{\text{st},\phi}, K_{\text{st},\mu})$. The topology of the equilibrium branch and our choice $\sigma = -1$ imply that $\partial_s \mu_{\text{eq}}(s_0) < 0$ and $\partial_s \phi_{\text{eq}}(s_0) < 0$. Thus, our criterion for stabilizing gains (assuming that ϕ is really governed by a scalar ODE when applying control), (3.40), requires that (ignoring the $O(\epsilon)$ terms)

$$(5.3) \quad K_{\text{st},\mu} < -\lambda_c < 0, \quad K_{\text{st},\phi} > -\frac{\partial_s \mu_{\text{eq}}(s_0)}{\partial_s \phi_{\text{eq}}(s_0)} K_{\text{st},\mu} > \frac{\partial_s \mu_{\text{eq}}(s_0)}{\partial_s \phi_{\text{eq}}(s_0)} \lambda_c > 0.$$

These estimates provide a lower bound on the gain $K_{\text{st},\phi}$ depending on the slope of the equilibrium branch and the degree of instability. So, we have to choose $K_{\text{st},\phi}$ positive and sufficiently large, and $K_{\text{st},\mu}$ negative and sufficiently large in modulus (larger than the instability λ_c). Figure 5.4 shows the evolution of the flow when feedback control through parameter is applied with a range of gains satisfying these (only necessary) criteria. We fix $K_{\text{st},\phi} = 2$ and vary $K_{\text{st},\mu} < 0$. The slope of the line $\{u = 0\}$ (dashed magenta) indicates the ratio between the gains. The reference point is $(\mu_{\text{pred},j}, \phi_{\text{pred},j}) = (0.0895, 0.06) \approx (0, 0)$ and is depicted with a black circle. The system shows large-amplitude oscillations around the line $u = 0$, jumping between the stable branches of equilibria. The fluctuations of the flux measure ϕ cause large and rapid excursions in parameter μ . For larger gains the projection of the flow follows the line $\{u = 0\}$ more closely. However, inherent fluctuations cause correction of the obstacle position that are larger than the corridor width (not shown in Figure 5.4). The criteria (5.3) are necessary, but they are sufficient only under Assumption 3.2 that the system to be controlled has only a single slow dimension with all others being strongly stable, made in

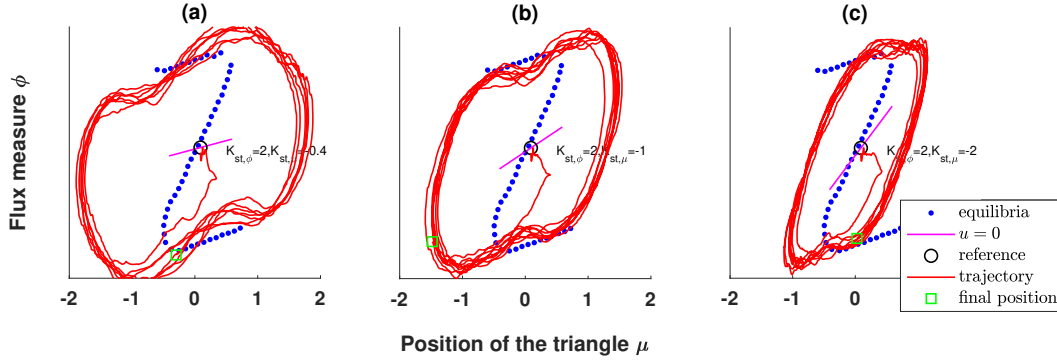


Figure 5.4. Results of the control through the bifurcation parameter close to the symmetric case of the corridor $(\mu_{\text{pred},j}, \phi_{\text{pred},j}) = (0.0895, 0.06)$, for different slopes of the line $u = 0$. The equilibria as computed by the zero-in-equilibrium feedback control are plotted in blue. The line $u = 0$ is plotted in magenda and the reference point with a black circle. The evolution of the system in phase space is plotted in red. For $K_{\text{st},\mu} < 0$ and fixed $K_{\text{st},\phi} = 2$ such that $u=0$ intersects the equilibrium line with the proper angle (see the discussion in 3.4.1), the system oscillates around the control line $u = 0$, jumping between the stable branches. It fails to approach the intersection of the line $u = 0$ and the equilibrium curve to converge to it as the small fluctuation in the pedestrian flow drives the system away from the unstable equilibrium.

subsection 3.4. Figure 5.4 gives evidence that this assumption is violated for gains satisfying (5.3).

6. Discussion and outlook. In this paper, we give a first outline for a general design principle for inherently non-invasive feedback control laws. These laws can be used to perform bifurcation analysis and track equilibria of dynamical systems that are not given in closed form. Instead we assume that we have an output of an experiment or a macroscopic quantity extracted from a microscopically defined dynamical system. A first result is that we devised a generalization of two well-known non-invasive feedback control laws, namely (a) feedback control with washout filter, which introduces a state observer, and (b) feedback control through the bifurcation parameter, calling our control law zero-in-equilibrium feedback control.

The proposed modification allows for continuous tracking of equilibria in the case of single-parameter studies and, more generally, can be seen as an improvement to the existing methodology as it requires a non-degeneracy condition that fails only at events of codimension $n_x + 1$, where n_x is the dimension of the reconstructed state that the feedback control can use. On the contrary, both feedback control with washout filters and feedback control through the bifurcation parameter fail at codimension-one events. Thus, failure becomes generic in single-parameter studies.

We have demonstrated the effectiveness of our feedback control law, the zero-in-equilibrium feedback control, on a particle model for a pedestrian evacuation scenario. For this system, we succeeded in tracking an entire branch of macroscopic equilibria through two macroscopic saddle-node bifurcation points, thus providing evidence that macroscopic bifurcations and

unstable states are behind the observed hysteresis and bistability for the particle model. Therefore, our feedback law holds promise also for a successful implementation in a physical experiment, which is much harder to re-initialize after failure of control than computational models. While we assumed the existence of a low-dimensional model during the design of the feedback control, the results can validate this assumption a-posteriori: convergence of the controlled system and vanishing control input ensure that the phenomenon observed is natural for the uncontrolled system. This is in contrast to analyzing a derived macroscopic model, as this derivation would be based on assumptions that may be hard to validate in states that cannot be observed in the uncontrolled system due to their dynamical instability or sensitivity.

Outlook for experiments. As the particle model explicitly included an alignment tendency among pedestrians moving in similar directions (see (4.3)), a natural next step are controlled physical experiments on pedestrian flows with real humans and data collection. These experiments will show when such an alignment tendency and the resulting bistability are really present, which we expect to depend strongly on the situation. The experiment will require manufacture of an obstacle that permits real-time adjustment of its position and an implementation of a bias force for subset of pedestrians in front of the obstacle. The analysis of the physical experiment would in turn lead to validation of high-dimensional particle models with multi-scale interactions, and understanding human pedestrian flows in real life.

More general inherently non-invasive control design principle. The zero-in-equilibrium feedback control is clearly not the most general possible formulation for inherently non-invasive feedback control. First, multiple control inputs may be practical when applying the feedback to computational experiments, as it may permit simpler design of control gains. Second, additional integral components (similar to x_{wo}), can be used to enforce constraints on the stabilized equilibrium that either detect or suppress a bifurcation. As a simple illustrative example, let us consider a limitation of the zero-in-equilibrium feedback control. The system (3.19) is not controllable in a pitchfork bifurcation point of a system with reflection symmetry. However, we can use additional integral components to enforce the symmetry. For example, for a system with, e.g., reflection symmetry R ($Rf(x, \mu, 0) = f(Rx, \mu, 0)$) we may formulate a non-invasive feedback law of the form

$$(6.1) \quad \dot{x} = f(x, \mu, a_u u + a_{\text{wo}} x_{\text{wo}}), \quad \dot{\mu} = u, \quad \dot{x}_{\text{wo}} = p^\top [R - I]x$$

with $\dim u = \dim x_{\text{wo}} = 1$, weights $a_u, a_{\text{wo}} \in \mathbb{R}$, and $p \in \mathbb{R}^{n_x}$ such that the tangent to the asymmetric branch is not orthogonal to p . One may easily check, that this system is controllable in the pitchfork bifurcation point $(x, \mu) = (0, 0)$ for the normal form example $f(x, \mu, u) = \mu x + x^3 + u$ with symmetry $Rx = -x$ and $p = 1$. The key assumption is that the control input is able to break the symmetry ($p^\top [R - I]f_u \neq 0$). Thus, feedback control laws designed for (6.1) would permit continuation of symmetric branches through a pitchfork bifurcation. This simple illustration shows that more general bifurcation control is possible. Of particular interest is control for periodic orbits of autonomous systems. While reduction to a discrete system through a Poincaré map should give straightforward results, this may not be the most practical approach for a system with large disturbances. Consequently, it would be interesting to revisit time-delayed feedback control to see if it can also be formulated in a way similar to the zero-in-equilibrium feedback control.

Acknowledgments. Jan Sieber’s research was supported by the UK Engineering and Physical Sciences Research Council (EPSRC) grants EP/N023544/1 and EP/V04687X/1. Jens Starke’s research was supported by the DFG (Deutsche Forschungsgemeinschaft) through the Collaborative Research Center CRC 1270, Grant/Award Number: SFB 1270/1-299150580.

REFERENCES

- [1] E. H. ABED, H. O. WANG, AND R. C. CHEN, *Stabilization of period doubling bifurcations and implications for control of chaos*, Physica D, 70 (1994), pp. 154–164.
- [2] E. L. ALLGOWER AND K. GEORG, *Numerical Continuation Methods: an Introduction*, vol. 13, Springer Science & Business Media, 2012.
- [3] K. J. ÅSTRÖM AND R. M. MURRAY, *Feedback systems*, Princeton University Press, 2010.
- [4] D. A. BARTON, *Control-based continuation: Bifurcation and stability analysis for physical experiments*, Mechanical Systems and Signal Processing, 84 (2017), pp. 54–64.
- [5] D. A. BARTON, B. P. MANN, AND S. G. BURROW, *Control-based continuation for investigating nonlinear experiments*, Journal of Vibration and Control, 18 (2012), pp. 509–520, <https://doi.org/10.1177/1077546310384004>.
- [6] D. A. W. BARTON AND J. SIEBER, *Systematic experimental exploration of bifurcations with noninvasive control*, Phys. Rev. E, 87 (2013), p. 052916, <https://doi.org/10.1103/PhysRevE.87.052916>.
- [7] A. S. BAZANELLA, P. V. KOKOTOVIC, AND A. S. E SILVA, *On the control of dynamic systems with unknown operating point*, in 1997 European Control Conference (ECC), IEEE, 1997, pp. 3434–3439.
- [8] E. BUREAU, F. SCHILDER, I. F. SANTOS, J. J. THOMSEN, AND J. STARKE, *Experimental bifurcation analysis of an impact oscillator—tuning a non-invasive control scheme*, Journal of Sound and Vibration, 332 (2013), pp. 5883–5897.
- [9] T. CHIN, J. RUTH, C. SANFORD, R. SANTORELLA, P. CARTER, AND B. SANDSTEDTE, *Enabling equation-free modeling via diffusion maps*, arXiv preprint arXiv:2112.15159, (2021).
- [10] R. R. COIFMAN, I. G. KEVREKIDIS, S. LAFON, M. MAGGIONI, AND B. NADLER, *Diffusion maps, reduction coordinates, and low dimensional representation of stochastic systems*, Multiscale Modeling & Simulation, 7 (2008), pp. 842–864.
- [11] H. DANKOWICZ AND F. SCHILDER, *Recipes for Continuation*, Computer Science and Engineering, SIAM, 2013.
- [12] E. J. DOEDEL, A. R. CHAMPNEYS, T. F. FAIRGRIEVE, Y. A. KUZNETSOV, B. SANDSTEDTE, X. WANG, ET AL., *Continuation and bifurcation software for ordinary differential equations (with homcont)*, AUTO97, Concordia University, Canada, (1997).
- [13] R. C. DORF AND R. H. BISHOP, *Modern control systems*, Pearson Prentice Hall, 2008.
- [14] D. GIVON, R. KUPFERMAN, AND A. STUART, *Extracting macroscopic dynamics: model problems and algorithms*, Nonlinearity, 17 (2004), p. R55.
- [15] W. J. GOVAERTS, *Numerical methods for bifurcations of dynamical equilibria*, SIAM, 2000.
- [16] T. GROSS, C. J. D. D’LIMA, AND B. BLASIUS, *Epidemic dynamics on an adaptive network*, Phys. Rev. Lett., 96 (2006), p. 208701, <https://doi.org/10.1103/PhysRevLett.96.208701>.
- [17] T. GROSS AND I. G. KEVREKIDIS, *Robust oscillations in sis epidemics on adaptive networks: Coarse graining by automated moment closure*, EPL (Europhysics Letters), 82 (2008), p. 38004.
- [18] M. A. HASSOUNEH, H.-C. LEE, AND E. H. ABED, *Washout filters in feedback control: Benefits, limitations and extensions*, in Proceedings of the 2004 American control conference, vol. 5, IEEE, 2004, pp. 3950–3955.
- [19] D. HELBING AND P. MOLNÁR, *Social force model for pedestrian dynamics*, Phys. Rev. E, 51 (1995), pp. 4282–4286, <https://doi.org/10.1103/PhysRevE.51.4282>.
- [20] P. HÖVEL, *Control of complex nonlinear systems with delay*, Springer Science & Business Media, 2010.
- [21] I. G. KEVREKIDIS AND G. SAMAIEY, *Equation-free multiscale computation: Algorithms and applications*, Annual Review of Physical Chemistry, 60 (2009), pp. 321–344, <https://doi.org/10.1146/annurev.physchem.59.032607.093610>. PMID: 19335220.
- [22] Y. KEVREKIDIS AND G. SAMAIEY, *Equation-free modeling*, Scholarpedia, 5 (2010), p. 4847, <https://doi.org/10.4236/scholarpedia.504847>.

- [org/10.4249/scholarpedia.4847](https://doi.org/10.4249/scholarpedia.4847). revision #91237.
- [23] I. Z. KISS, J. C. MILLER, AND P. L. SIMON, *Mathematics of epidemics on networks: From exact to approximate models*, vol. 46 of Interdisciplinary Applied Mathematics, Springer International Publishing, Cham, 2017, <https://doi.org/10.1007/978-3-319-50806-1>.
- [24] Y. A. KUZNETSOV, *Elements of Applied Bifurcation Theory*, vol. 112 of Applied Mathematical Sciences, Springer-Verlag, New York, third ed., 2004.
- [25] Y. LI AND H. DANKOWICZ, *Adaptive control designs for control-based continuation of periodic orbits in a class of uncertain linear systems*, *Nonlinear Dynamics*, 103 (2021), pp. 2563–2579.
- [26] C. MARSCHLER, J. SIEBER, R. BERKEMER, A. KAWAMOTO, AND J. STARKE, *Implicit methods for equation-free analysis: convergence results and analysis of emergent waves in microscopic traffic models*, *SIAM Journal on Applied Dynamical Systems*, 13 (2014), pp. 1202–1238.
- [27] S. MISRA, H. DANKOWICZ, AND M. R. PAUL, *Event-driven feedback tracking and control of tapping-mode atomic force microscopy*, *Proceedings of the Royal Society A: Mathematical, Physical and Engineering Sciences*, 464 (2008), pp. 2113–2133.
- [28] P. MOLNÁR AND J. STARKE, *Control of distributed autonomous robotic systems using principles of pattern formation in nature and pedestrian behavior*, *IEEE Transactions on Systems, Man, and Cybernetics, Part B (Cybernetics)*, 31 (2001), pp. 433–435.
- [29] L. PELLIS, T. HOUSE, AND M. J. KEELING, *Exact and approximate moment closures for non-Markovian network epidemics*, *Journal of Theoretical Biology*, 382 (2015), pp. 160–177, <https://doi.org/10.1016/j.jtbi.2015.04.039>.
- [30] K. PYRAGAS, *Continuous control of chaos by self-controlling feedback*, *Physics Letters A*, 170 (1992), pp. 421 – 428, [https://doi.org/10.1016/0375-9601\(92\)90745-8](https://doi.org/10.1016/0375-9601(92)90745-8).
- [31] K. PYRAGAS, V. PYRAGAS, I. Z. KISS, AND J. L. HUDSON, *Adaptive control of unknown unstable steady states of dynamical systems*, *Phys. Rev. E*, 70 (2004), p. 026215, <https://doi.org/10.1103/PhysRevE.70.026215>.
- [32] S. F. RAILSBACK AND V. GRIMM, *Agent-based and individual-based modeling: a practical introduction*, Princeton University Press, Princeton and Oxford, 2019.
- [33] M. SCHEFFER, *Critical Transitions in Nature and Society*, Princeton University Press, Princeton and Oxford, 2009.
- [34] F. SCHILDER, E. BUREAU, I. F. SANTOS, J. J. THOMSEN, AND J. STARKE, *Experimental bifurcation analysis—continuation for noise-contaminated zero problems*, *Journal of Sound and Vibration*, 358 (2015), pp. 251–266.
- [35] J. SIEBER, A. GONZALEZ-BUELGA, S. A. NEILD, D. J. WAGG, AND B. KRAUSKOPF, *Experimental continuation of periodic orbits through a fold*, *Phys. Rev. Lett.*, 100 (2008), p. 244101, <https://doi.org/10.1103/PhysRevLett.100.244101>.
- [36] J. SIEBER, C. MARSCHLER, AND J. STARKE, *Convergence of equation-free methods in the case of finite time scale separation with application to deterministic and stochastic systems*, *SIAM Journal on Applied Dynamical Systems*, 17 (2018), pp. 2574–2614, <https://doi.org/10.1137/17M1126084>.
- [37] C. SIETTOS, C. GEAR, AND I. KEVREKIDIS, *An equation-free approach to agent-based computation: Bifurcation analysis and control of stationary states*, *EPL (Europhysics Letters)*, 99 (2012), p. 48007.
- [38] C. I. SIETTOS, D. MAROUDAS, AND I. G. KEVREKIDIS, *Coarse bifurcation diagrams via microscopic simulators: a state-feedback control-based approach*, *International Journal of Bifurcation and Chaos*, 14 (2004), pp. 207–220.
- [39] A. SINGER, R. ERBAN, I. G. KEVREKIDIS, AND R. R. COIFMAN, *Detecting intrinsic slow variables in stochastic dynamical systems by anisotropic diffusion maps*, *Proceedings of the National Academy of Sciences*, 106 (2009), pp. 16090–16095.
- [40] J. STARKE, K. B. THOMSEN, A. SØRENSEN, C. MARSCHLER, F. SCHILDER, A. DEDERICHS, AND P. HJORTH, *Nonlinear effects in examples of crowd evacuation scenarios*, in 17th International IEEE Conference on Intelligent Transportation Systems (ITSC), Oct 2014, pp. 560–565, <https://doi.org/10.1109/ITSC.2014.6957749>.
- [41] A. TSOUMANIS AND C. SIETTOS, *Detection of coarse-grained unstable states of microscopic/stochastic systems: a timestepper-based iterative protocol*, *Nonlinear Dynamics*, 67 (2012), pp. 103–117.
- [42] C. VANDEKERCKHOVE, B. SONDAY, A. MAKEEV, D. ROOSE, AND I. G. KEVREKIDIS, *A common approach to the computation of coarse-scale steady states and to consistent initialization on a slow manifold*,

Computers & Chemical Engineering, 35 (2011), pp. 1949 – 1958.

- [43] H. O. WANG AND E. H. ABED, *Bifurcation control of a chaotic system*, Automatica, 31 (1995), pp. 1213 – 1226, [https://doi.org/10.1016/0005-1098\(94\)00146-A](https://doi.org/10.1016/0005-1098(94)00146-A).

Appendix A. Parameter values for model and methods.

Model parameters. Table A.1 shows all parameters entering the social force model with alignment, defined in Equations (4.1)–(4.4), Table A.2 lists parameters entering pedestrian flux measures Φ_{\pm} and ϕ , defined in Equations (4.7)–(4.8), and Table A.3 lists parameters entering the input effect, b , given in (4.10).

Parameter	Symbol	Value	Units
Corridor length	C_{len}	20	m
Corridor width	C_{wth}	10	m
Number of pedestrians	N	100	-
Triangular obstacle's base side	L_{base}	4	m
Triangular obstacle's leg sides	L_{iso}	3	m
Preferred walking speed	v_{trg}	1.34	ms^{-1}
Target point for walking	\mathbf{x}_{trg}	(0, 20)	(m, m)
Reaction time of pedestrians	τ	0.22	s
Pedestrian-pedestrian repulsion	$V_{\text{rep},ij}^{\text{ped}}$	15	m^2s^{-2}
Pedestrian-pedestrian length scale	σ^{ped}	1	m
Pedestrian-Obstacle repulsion	$V_{\text{rep},ij}^{\text{obj}}$	10	m^2s^{-2}
Pedestrian-Obstacle length scale	σ^{obj}	2	m
Lemming effect parameter	p_{al}	0.75	-
Weight function κ scaling factor	γ	$\exp(1)$	-
Weight function κ angle scale	β	0.9	-
Weight function κ angle scale magnitude	α	15	-
Weight function κ length scale	δ	5	m

Table A.1

Model parameters for Equations (4.1)–(4.4), see also Figure 4.1 for meaning of geometry parameters for corridor and obstacle.

Numerical integration details for simulation of social force model with alignment. For all simulations, we use the *MATLAB* ode45-solver with a fixed step size of 0.1 sec. Throughout the simulation, $N = 100$ pedestrians/particles were always inside the corridor. To this end, an event function was implemented. This function detects when a particle has left the corridor or, equivalently, when for a particle i with positions (x_i, y_i) it holds that $y_i > C_{\text{len}}/2$. In that event, the differential equations that correspond to particle i are removed from the integrated system and a new particle i is injected at the other side of the corridor. The new particle enters with $y_i = -C_{\text{len}}/2$ and with a vertical position x_i uniformly random distributed around the center line of the corridor within the interval $[-0.5, 0.5]$ m. The initial velocity is $(v_{\text{trg}}, 0)$.

Parameter	Symbol	Value	Units
(Φ_{\pm}) half-length (in y) of box in Figure 4.3b	$y_{\text{len},\Phi}$	0.5	m
(Φ_{\pm}) center (in y) of box in Figure 4.3b	$y_{c,\Phi}$	2.75 ^[*]	m
(Φ_{\pm}) length of interval for time averaging	τ_{max}	10	sec
(ϕ) length scale of w_{pos}	d	4	m
(ϕ) scaling factor/dimension of flux	η	1/12	s/m ³
(ϕ) distance of extrema for w_{pos} from middle of corridor	$x_{c,\phi}$	$C_{\text{wth}}/2 = 5$	m
(ϕ) location of extrema for w_{pos} along corridor	$y_{c,\phi}$	0	m

Table A.2

Parameters, defining output measures, time-averaged fluxes Φ_{\pm} and space-averages flux ϕ in (4.7), (4.8), see also [Figure 4.3b](#) for illustration of graph for w_{pos} and box location for Φ_{\pm} . [*] The value of $y_{c,\Phi}$ is determined as $\sqrt{L_{\text{iso}}^2 - L_{\text{base}}^2}/4 + 0.5 = \sqrt{5} + 0.5 \approx 2.75$

Parameter	Symbol	Value	Units
half-length (in y) of box for feedback input	$y_{\text{len},b}$	0.25	m
half-width (in x) of box for feedback input	$x_{\text{wth},b}$	$C_{\text{wth}}/3 = 3.3$	m
center (in y) of box for feedback input	$y_{c,b}$	-1.75	m
center (in x) of box for feedback input	$x_{c,b}$	μ	m

Table A.3

Parameters, defining input support box for b , where the feedback control u can act, defined in (4.9), (4.10), see also [Figure 4.3a](#) for illustration of the location of the box relative to corridor and obstacle.